#### **OPEN ACCESS**



# Two-process Model and Residual Abundance Analysis of the Milky Way Massive Satellites

Sten Hasselquist <sup>1</sup>, Christian R. Hayes <sup>1,2</sup>, Emily J. Griffith <sup>3</sup>, David Weinberg <sup>4</sup>, Tawny Sit <sup>5</sup>, Rachael L. Beaton <sup>1,6</sup>, and Danny Horta <sup>7</sup>

<sup>1</sup> Space Telescope Science Institute, 3700 San Martin Drive, Baltimore, MD 21218, USA

### **Abstract**

The "two-process model" is a promising technique for interpreting stellar chemical abundance data from large-scale surveys (e.g., the Sloan Digital Sky Survey IV/V and the Galactic Archeology with HERMES survey), enabling more quantitative empirical studies of differences in chemical enrichment history between galaxies without relying on detailed yield and evolution models. In this work, we fit two-process model parameters to (1) a luminous giant Milky Way (MW) sample and (2) stars comprising the Sagittarius dwarf galaxy (Sgr). We then use these two sets of model parameters to predict the abundances of 14 elements of stars belonging to the MW and in five of its massive satellite galaxies, analyzing the residuals between the predicted and observed abundances. We find that the model fit to (1) results in large residuals (0.1–0.3 dex) for most metallicity-dependent elements in the metal-rich ([Mg/H] > -0.8) stars of the satellite galaxies. However, the model fit to (2) results in small or no residuals for all elements across all satellite galaxies. Therefore, despite the wide variation in [X/Mg]–[Mg/H] abundance patterns of the satellite galaxies, the two-process framework provides an accurate characterization of their abundance patterns across many elements, but these multielement patterns are systematically different between the dwarf galaxy satellites and the MW disks. We consider a variety of scenarios for the origin of this difference, highlighting the possibility that a large inflow of pristine gas to the MW disk diluted the metallicity of star-forming gas without changing abundance ratios.

Unified Astronomy Thesaurus concepts: Galaxy chemical evolution (580); Chemical abundances (224)

# 1. Introduction

Understanding the detailed chemical abundance patterns for individual stars in a galaxy is essential for understanding their detailed histories of star formation, accretion, and outflows for the subset of galaxies where such measurements can be obtained. The nucleosynthetic sites and timescales for element production are known for many chemical elements, and thus the details of the star formation history (SFH) of a galaxy can be inferred from its detailed chemical abundance patterns. For example, the abundance of the  $\alpha$  elements (O, Mg, Si, S, and Ca) as measured relative to the abundance of a heavier element, such as Fe (often expressed as  $[\alpha/\text{Fe}]$ ), can provide some estimate of the star formation efficiency of a galaxy, with elevated or increasing abundance ratios indicating times of relatively vigorous star formation and deficient or decreasing abundance ratios signaling times of less vigorous star formation, with delayed Type Ia supernovae (SNe Ia) becoming more prominent sources of chemical enrichment (e.g., B. M. Tinsley 1979; B. Edvardsson et al. 1993; M. Shetrone et al. 2003; B. Hendricks et al. 2014; D. L. Nidever et al. 2020; S. Hasselquist et al. 2021). The abundances of the

Original content from this work may be used under the terms of the Creative Commons Attribution 4.0 licence. Any further distribution of this work must maintain attribution to the author(s) and the title of the work, journal citation and DOI.

elements produced in large quantities by the s-process in asymptotic giant branch (AGB) stars can indicate the relative contribution of these stars to the chemical evolution of a galaxy or globular cluster (GC; e.g., B. M. Tinsley 1979; C. Kobayashi et al. 2006, 2020a). Measuring abundance ratios of the elements produced in hydrostatic burning to those produced in explosive synthesis can probe some details of the initial mass function (IMF) of a galaxy at the time at which it formed those stars (e.g., A. McWilliam et al. 2013; S. Hasselquist et al. 2017; J. L. Carlin et al. 2018; A. P. Ji et al. 2020). Further detailed abundance patterns of even more elements can reveal aspects of stochastic sampling of the IMF (e.g., A. Koch et al. 2008; A. P. Ji et al. 2020; E. J. Griffith et al. 2023) and/or assist in our understanding of the exact nature of less well-understood enrichment sources, such as the sources of the r-process (e.g., C. Sneden et al. 2008; A. P. Ji et al. 2016; J. Lian et al. 2023).

Despite numerous studies that have advanced our knowledge of how specific details of the SFH vary with galaxy mass and environment, powerful quantitative interpretations remain elusive. Ideally, one could use a parameterized chemical evolution model to fit multielement abundances, each of which is sensitive to different aspects of an SFH. Such efforts, while important and insightful, generally find that not every chemical element is able to be accurately predicted in the MW (see, e.g., B. H. Andrews et al. 2017; J. Rybizki et al. 2017; C. Kobayashi et al. 2020a). The failures are likely some combination of the abundance measurements themselves (e.g., not including

<sup>&</sup>lt;sup>2</sup> Herzberg Astronomy and Astrophysics Research Centre, Victoria, BC V9E 2E7, Canada

<sup>&</sup>lt;sup>3</sup> Center for Astrophysics and Space Astronomy, Department of Astrophysical and Planetary Sciences, University of Colorado, 389 UCB, Boulder, CO 80309-0389, USA

<sup>&</sup>lt;sup>4</sup> The Department of Astronomy and Center of Cosmology and AstroParticle Physics, The Ohio State University, Columbus, OH 43210, USA

<sup>5</sup> Department of Astronomy, The Ohio State University, Columbus, OH 43210, USA

<sup>6</sup> Department of Physics and Astronomy, Johns Hopkins University, Baltimore, MD 21218, USA

<sup>7</sup> Center for Computational Astrophysics, Flatiron Institute, 162 5th Avenue, New York, NY 10010, USA

\*\*Received 2024 April 22; revised 2024 July 30; accepted 2024 August 17; published 2024 October 15

corrections for non-local thermodynamic equilibrium, or "NLTE"), incorrect or incomplete yield calculations, and unknown or exotic sources that are not explicitly accounted for in the models (e.g., sub-Chandrasekhar-mass SNe Ia; S. E. Woosley et al. 1994; A. McWilliam et al. 2018). These tools are further complicated by the fact that each study that measures abundances is typically affected by unconstrained systematic uncertainties, complicating how these abundance results are combined and compared.

One tool with the potential to better quantify and understand differences in the detailed SFH of galaxies is the "two-process model," which was first described in D. H. Weinberg et al. (2019) and applied to chemical abundance measurements from hundreds of thousands of Milky Way (MW) stars observed by the Apache Point Observatory Galaxy Evolution Experiment (APOGEE; S. R. Majewski et al. 2017). The major assumption of this model is that every chemical abundance in a star can be described as the sum of contributions to this element from a "prompt" process (typically assigned to Type II or "corecollapse supernovae," CCSNe) and a "delayed" process (typically assigned to SNe Ia). They divided the MW into two samples based on their [Fe/Mg]-[Mg/H] abundance patterns: the low-Ia (high- $\alpha$ ) sequence, which is a sequence comprised primarily or entirely by the prompt process, and the high-Ia (low- $\alpha$ ) sample, which is a sequence that formed from contributions from both processes. From the observed trends of [X/Mg] versus [Mg/H] within these two populations, they inferred model parameters describing the relative contribution of each process to the observed elements. X. D. H. Weinberg et al. (2019) then used this model to predict the abundances of the other elements measured by APOGEE, confirming that the abundance patterns of these sequences for virtually all of these elements are identical throughout the Galactic disk (see also, e.g., D. L. Nidever et al. 2014; M. R. Hayden et al. 2015), with follow-up works confirming that these chemical similarities extend to the Galactic bulge and inner Galaxy (e.g., G. Zasowski et al. 2019; E. Griffith et al. 2021). E. J. Griffith et al. (2022) found that the two-process model is able to do similarly well in predicting the abundances of MW stars that have abundances derived from the Galactic Archeology with HERMES survey (A. Sheinis et al. 2015) data release 3 (DR3; S. Buder et al. 2021) rather than APOGEE, obtaining similar results for elements common to both surveys and extending the two-process model to elements not measured by APOGEE.

It is worth emphasizing that the two-process model is not expected to be a perfect description of high-dimensional abundance patterns; if anything, its accuracy in fitting these patterns in the MW disk and bulge is a surprise. The fact that the detailed abundance patterns of nearly all MW stars are well fit by the two-process model implies that the nucleosynthetic processes creating the elements and dispersing them throughout the interstellar medium (ISM) of the MW were largely invariant with time and Galactic location. In other words, the IMFaveraged yields of each process appear to result in the same chemical abundances at fixed metallicity ([Mg/H]) and relative contribution from each process (as traced by [Fe/Mg]). However, the small element-by-element residuals from a twoparameter description are statistically significant (D. H. Weinberg et al. 2022; Y.-S. Ting & D. H. Weinberg 2022; B. L. Ratcliffe & M. K. Ness 2023) and some stars observed by APOGEE show much larger residuals. Specifically, D. H. Weinberg et al.

(2022) showed that stars belonging to the LMC and  $\omega$  Cen exhibit large residuals between the observed and model-predicted abundances for many elements, a result confirmed and extended to other MW satellite galaxies by T. Sit et al. (2024) with a much larger sample after taking into account potential systematic abundance measurement errors. The magnitude, detailed form, and environmental dependence of these residuals from the two-process model can provide empirical clues about enrichment processes and their impact on different galaxies and Galactic components.

Analyzing and interpreting these empirical clues remains a difficult task as it is still an open question as to whether these two-process model abundance residuals indicate differences in the element yields of the prompt or delayed process in different systems, the role of a third or fourth process that has different relative amplitude in these systems, or a more fundamental breakdown of the assumptions that lead to the two-process description in the first place. For example, we might expect elements primarily produced in AGB stars to show large twoprocess model residuals for dwarf galaxies (DGs) that are known to have had a significant contribution to their chemical enrichment from AGB stars, as this process is not separately accounted for in the two-process model. However, for the elements in the MW that appear to be accurately predicted via a combination of CCSNe and SNe Ia, large two-process model residuals in extragalactic systems taken at face value suggest actual differences in the IMF-averaged yields of one or both types of SNe. Of course, such differences need not necessarily imply differences in stellar astrophysics, as the residuals could be revealing a flaw in the model assumptions that are more obvious in systems with different galactic evolution. Therefore, a more in-depth study of what these residuals actually mean is warranted.

Moreover, it is still unknown if the DG residual abundance patterns found in T. Sit et al. (2024) are shared across all DGs, or if each galaxy exhibits its own unique residual abundance pattern. Stated more generally, are the residual abundance patterns of the DGs indicative of a fundamental difference in how an MW-sized galaxy is formed versus a DG, or do the residual abundance patterns of each depend uniquely on mass and environment? S. Hasselquist et al. (2021) attempted to answer this question without making use of the two-process model, finding that, while the  $\alpha$ -element abundance patterns implied vast differences in the star formation rate as a function of time between these galaxies, the detailed abundance patterns of the other elements were much more difficult to interpret. For many elements observed in these galaxies, it was inconclusive if the variation in abundance patterns were signals of fundamental differences between the chemical enrichment processes that occurred, or like in the MW, the abundance patterns are what are expected given the ratio of a prompt process to a delayed process, as traced by the [Mg/H] and [Fe/Mg] abundances of each galaxy.

In this work, we carefully select a MW sample that matches the stellar parameters of the satellite galaxy sample of S. Hasselquist et al. (2021), and derive two separate sets of abundance vectors for the two-process model, creating a "MW two-process model" and a "DG two-process model." We then use both models to predict the chemical abundances of the satellite galaxies, linking residuals to potential real differences in the detailed chemical evolution of these galaxies, issues with the two-process model assumptions, or both. The data used and

target selection are described in Section 2. The two-process model and how we fit the model parameters are described in Section 3. The model parameters that we derive are discussed in Section 4. Residual abundance results are presented in Section 5 and discussed in Section 6.

#### 2. Data and Target Selection

We use observations from the Apache Point Observatory Galactic Evolution Experiment (APOGEE; S. R. Majewski et al. 2017), which was a near-infrared spectroscopic survey of hundreds of thousands of stars across the MW as part of the third and fourth iterations of the Sloan Digital Sky Survey (SDSS-III; D. J. Eisenstein et al. 2011 and SDSS-IV; M. R. Blanton et al. 2017). The APOGEE survey used two nearly identical spectrographs (J. C. Wilson et al. 2019), one on the SDSS 2.5 m telescope at Apache Point Observatory (J. E. Gunn et al. 2006) and another on the 2.5 m du Pont telescope at Las Campanas Observatory (I. S. Bowen & A. H. Vaughan 1973).

Throughout the lifetime of these surveys, the APOGEE spectrographs obtained high-resolution ( $R \sim 22,000$ ) H-band spectra of nearly 750,000 stars distributed throughout the MW and its nearby satellite galaxies (targeting descriptions are given in G. Zasowski et al. 2013, 2017, F. A. Santana et al. 2021, and R. L. Beaton et al. 2021), from which stellar parameters and detailed chemical abundances were obtained using the APOGEE Stellar Parameters and Chemical Abundance Pipeline (ASPCAP; A. E. García Pérez et al. 2016). ASPCAP uses the FERRE code (C. Allende Prieto et al. 2006) to match the normalized, radial-velocity-corrected, and sky-subtracted spectra (D. L. Nidever et al. 2015) to a library of synthetic stellar spectra (O. Zamora et al. 2015 with updates described in H. Jönsson et al. 2020), allowing for the determination of up to  $\sim$ 20 chemical abundances. In this work, we use data from Data Release 17 (Abdurro'uf et al. 2022), which includes NLTE calculations for Na, Mg, K, and Ca (Y. Osorio et al. 2020), along with Ce abundances from K. Cunha et al. (2017).

In this work, we analyze a sample of DGs studied in S. Hasselquist et al. (2021), which include the LMC, SMC, Sagittarius dwarf galaxy (Sgr), Fnx, and the large fraction of the MW halo that is believed to have come from a single progenitor galaxy (e.g., P. E. Nissen & W. J. Schuster 2010; A. Helmi et al. 2018; A. J. Deason et al. 2018; C. R. Hayes et al. 2018; V. Belokurov et al. 2018), which we refer to in this work as the Gaia Sausage/Enceladus galaxy (GSE). The selection of stars for each of these systems is described in detail by S. Hasselquist et al. (2021) and was based on Gaia DR2 proper motions (A. G. A. Brown et al. 2018), APOGEE radial velocities, distances, and orbital parameters from the astronn code (H. W. Leung & J. Bovy 2019), and, in the case of the MCs, additional photometric selections were made to exclude obvious AGB stars and massive supergiant stars.

We also select a MW sample that is used to derive the model parameters for the two-process model. Because of small APOGEE systematic abundance trends with effective temperature and surface gravity (see, e.g., H. Jönsson et al. 2020; E. Griffith et al. 2021; D. H. Weinberg et al. 2022; T. Sit et al. 2024), we are careful to select an MW sample that covers the same  $T_{\rm eff}$  and  $\log g$  distributions as the stars in the massive satellite sample. To select our MW sample, we first explicitly exclude the satellite galaxy members identified in

- S. Hasselquist et al. (2021), and then start with the following selection criteria:
  - 1. [Fe/H] < 0.2, as no DG has stars more metal-rich than this value.
  - 2.  $\log(g) < 3.0$ , as this removes obvious dwarf stars because main-sequence stars are too faint for APOGEE to observe at the distances of these satellite galaxies.
  - 3. Median signal-to-noise ratio per pixel > 80.
  - 4. Targeting flag EXTRATARG = 0 to ensure the sample does not include any "special targets," e.g., stars that were targeted based on their known or suspected membership in GCs. To be as complete as possible, we also remove any stars that have been identified by R. P. Schiavon et al. (2024) to be in GCs that may have been serendipitously targeted by APOGEE.

From this MW sample, which is comprised of  $\sim$ 30,000 stars, we then create two separate MW subsamples by randomly subselecting 10,000 MW stars that either match the  $T_{\rm eff}$ distribution (subsample 1) or match the  $\log g$  distribution (subsample 2) to that of the satellite galaxies. The distributions of stellar parameters for each of these selections, and how they compare to those of the satellite galaxy sample, are shown in Figure 1. In general, the satellite galaxy distributions are matched fairly well, but in the case of the  $\log g$  distribution, there are not quite enough MW stars at each log g to return an exact distribution. Moreover, the metallicity distribution of the MW  $T_{\rm eff}$ -matched sample is slightly more metal-poor than the log g-matched distribution. Therefore, we focus most of the results and analysis on the  $T_{\rm eff}$ -matched sample, showing some of the results from the  $\log g$ -matched sample in the Appendix. Our main results and conclusions are not sample dependent.

Because the APOGEE survey contains a relatively small fraction of stars at [Fe/H] < -0.65, we supplement the above 10,000 star MW sample with all stars observed by APOGEE with [Fe/H] < -0.65 that meet the above criteria with an additional criterion of  $\log g < 1.6$ . Of course, this results in a sample that is largely contaminated from GSE stars that were not included in the S. Hasselquist et al. (2021) sample, as their sample was focused on purity rather than completeness. Therefore, we mitigate GSE contamination in this metal-poor sample by enforcing the following additional cuts on these metal-poor stars:

- 1. [Fe/H] < -0.65 and [Mg/Fe] > 0.05.
- 2. [Fe/H] < -0.95 and [Mg/Fe] > 0.27.

The stellar parameter distributions of these stars are shown in the red-hatched histograms of Figure 1. To demonstrate exactly which stars we include at these low metallicities, we show in Figure 2 the [Mg/Fe]–[Fe/H] abundance plane for this MW metal-poor sample alongside each satellite galaxy sample. A global [Mg/Fe] offset of -0.05 is applied such that stars with solar [Fe/H] have [Mg/Fe] = 0.0. The left panel of Figure 2 shows that the metal-poor MW sample at [Mg/Fe] > 0.27 likely contains some amount of GSE contamination, particularly in the metallicity range -2.0 < [Fe/H] < -1.5. However, as long as the "pure CCSNe" abundances of a GSE star do not differ significantly from those of a pure CCSNe MW star, this should have a negligible effect on our results. It is more important that the metal-poor end of the MW low- $\alpha$  sequence does not contain

<sup>8</sup> See https://www.sdss4.org/dr17/irspec/targets/.

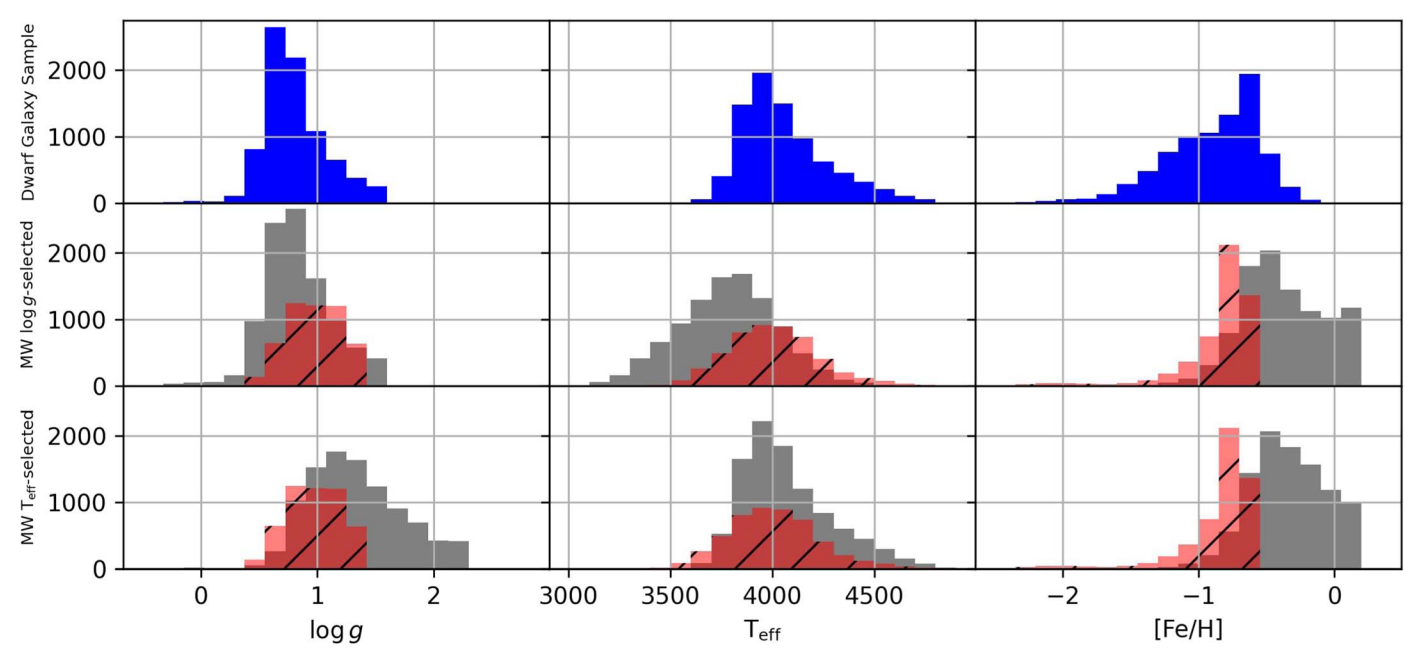


Figure 1. Stellar parameter distributions for the DG sample (top row) and MW selection subsamples (bottom two rows). The middle row shows the stellar parameters of the MW sample obtained by selecting stars such that the  $\log g$  distribution is the same as the DGs (subsample 1). The bottom row is the same as the second row, but matching on  $T_{\rm eff}$  (subsample 2). The MW "metal-poor" sample, as described in the text, is shown in the red-hatched distribution.

GSE contamination, as the most metal-rich GSE stars have a much lower [Mg/Fe] abundance than the most metal-poor MW stars (as shown in the third from left panel of Figure 2), which would cause us to fit two-process model parameters to a median that is perhaps in between these sequences (described in more detail in Figure 4). Moreover, as described in Section 5, our results that rely on the MW two-process model are limited to the metallicity range  $-1.0 < [{\rm Mg/H}] < 0.0$ , where the high-Ia MW sample overlaps with the satellite galaxies, and are thus not affected by potential GSE contamination. A more in-depth understanding of how the two-process model parameters and subsequent predictions are affected by the GSE/MW ambiguity at [Fe/H] < -1.5 can be found in E. J. Griffith et al. (2024, in preparation).

#### 3. The Two-process Model

The two-process model (described in detail in D. H. Weinberg et al. 2019 and D. H. Weinberg et al. 2022) is a tool to predict the chemical abundances of a star given its [Mg/Fe] and [Mg/H] abundances. The model assumes that the chemical abundance pattern of a star is a result of chemical enrichment from a prompt enrichment process and a delayed enrichment process, which can be physically linked to SNe II and SNe Ia, respectively. We note that the model is agnostic to what or how many physical mechanisms actually comprise the prompt and delayed enrichment processes. To "train" the model, one uses median abundance trends of low-Ia (a.k.a. high- $\alpha$ ) and high-Ia (a.k.a. low- $\alpha$ ) stars to derive two "process vectors" ( $q_{\rm cc}$  and  $q_{\rm Ia}$ ), which describe the IMF-averaged yields of each element within each process at a given metallicity. We derive these vectors in bins of size 0.1 dex in [Mg/H]. The predicted abundances of a given star depend on the amplitudes ( $A_{cc}$  and  $A_{Ia}$ ) of these two processes, which can be inferred from Mg and Fe alone or by fitting multiple elements. For detailed formulations of the model and its assumptions, we refer the reader to D. H. Weinberg et al. (2022) and E. J. Griffith et al. (2024).

The goals of this work are (1) to understand the extent to which a two-process model with parameters fit to the MW abundance patterns is able to predict the abundances of other galaxies and (2) to understand the extent to which a two-process model with parameters fit to a single DG (we choose Sgr) is able to predict the abundances of the other satellite galaxies. We therefore derive two sets of abundance vectors for each scenario. Inferring the model parameters by solving the abundance vector equations requires us to define two separate groups with distinct levels of SNe Ia enrichment at a given level of CCSNe enrichment. The division we use to define the "low-Ia" group is

- 1. Fe/H > -1.2 and [Mg/Fe]  $> 0.12-0.13^*$ [Fe/H] (same as D. H. Weinberg et al. 2019);
- 2. Fe/H > 0.0 and [Mg/Fe] > 0.12 (same as D. H. Weinberg et al. 2019); and
- 3. Fe/H <-1.2 and [Mg/Fe] >0.27 (introduced in this work).

We chose these divisions to be consistent with D. H. Weinberg et al. (2019) and D. H. Weinberg et al. (2022), where the metallicities of their sample overlap with ours, but introduce a new [Mg/Fe] division at [Fe/H] < -1.2 to select metal-poor stars that have [Mg/Fe] abundances close to the assumed "pure" prompt ratio of [Mg/Fe] = +0.3, described in detail below. Because we are ultimately fitting model parameters to the median trends of these samples, the exact placement of these divisions as well as whether we divide in the [Mg/Fe]-[Fe/H] abundance plane or the [Fe/Mg]-[Mg/H] abundance plane has little to no impact on the model parameters that we derive.

This low-Ia sample, which is assumed to contain chemical enrichment primarily or entirely from the prompt process, is plotted as orchid-colored points in Figure 3. For goal (1) listed above, the high-Ia sample used to infer the parameters is comprised of all MW stars selected in Section 2 that have [Mg/Fe] abundances below the above division, plotted as

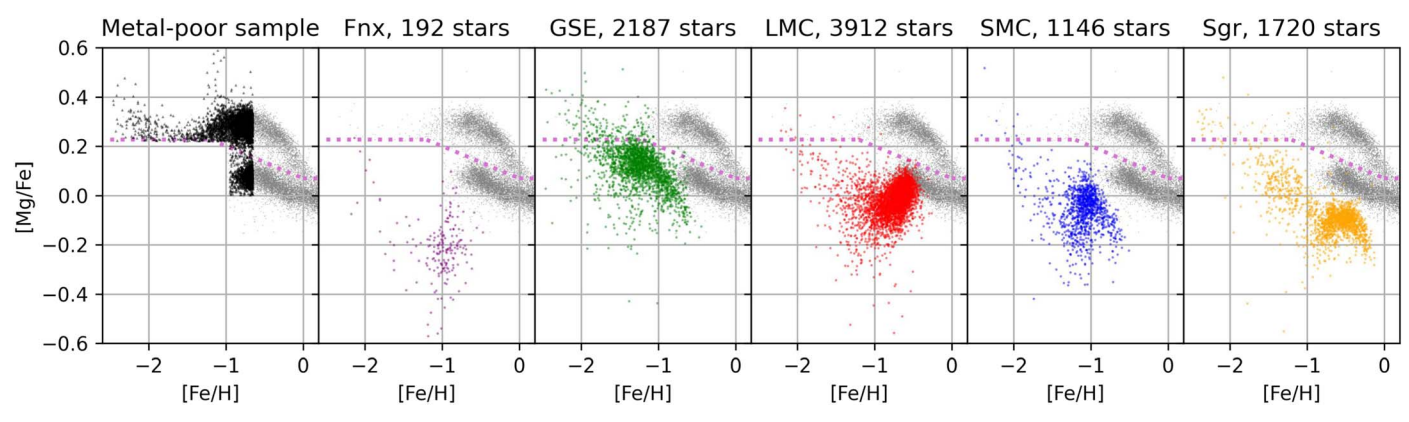


Figure 2. [Mg/Fe] vs. [Fe/H] for the metal-poor MW sample (described in the text) and the sample for each of the satellite galaxies (the latter follows S. Hasselquist et al. 2021). The MW  $T_{\text{eff}}$ -matched sample is reproduced in each panel as gray points. The number of stars in each sample is indicated in the title of each plot. A global [Mg/Fe] offset of -0.05 has been applied such that MW stars at solar [Fe/H] have [Mg/Fe] = 0.0.

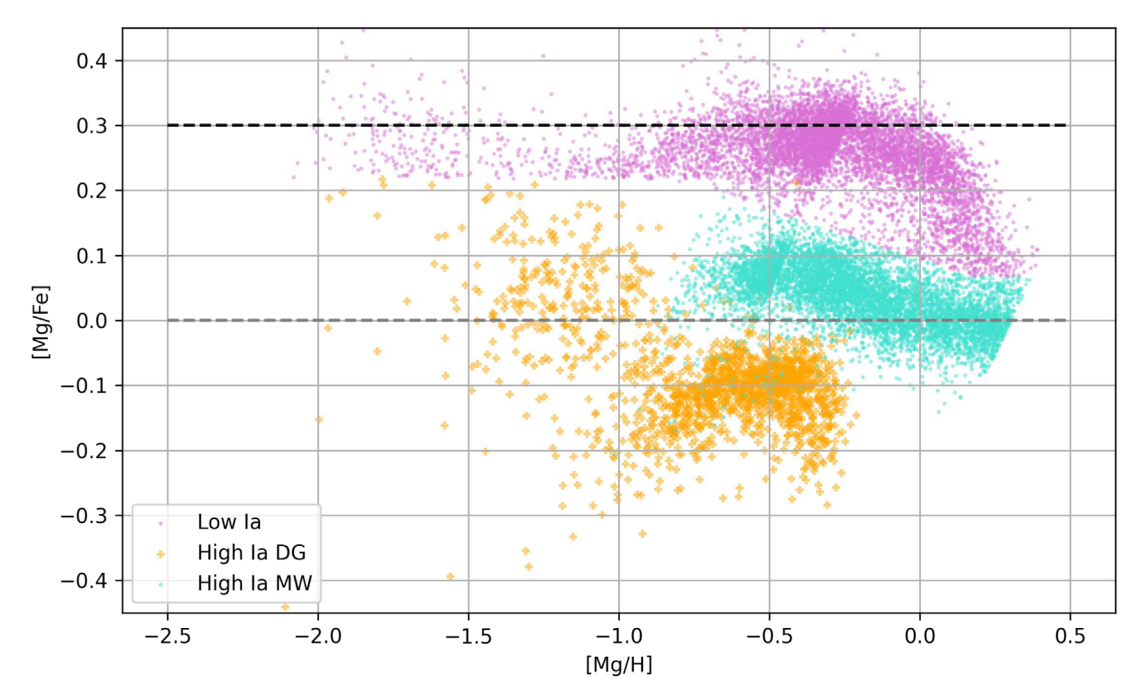


Figure 3. [Mg/Fe]-[Mg/H] abundance patterns for the MW low-Ia sample (orchid), MW high-Ia sample (turquoise), and DG high-Ia sample (orange). The black dashed horizontal line marks the assumed "pure" core-collapse Mg/Fe ratio of [Mg/Fe]=0.3. The gray dashed line marks the solar Mg/Fe ratio of [Mg/Fe]=0.0.

turquoise-colored points in Figure 3 and henceforth referred to as the "high-Ia MW" sample. For goal (2) listed above, the high-Ia sample is instead comprised of all Sgr stars that have [Mg/Fe] below the above division. We refer to this sample as the "high-Ia DG" sample to indicate that it is used to fit the model parameters with the goal of comparing to other DGs. We could have chosen any galaxy for goal (2), but decided to select Sgr because it spans the entire metallicity range of all satellite galaxies studied here, and unlike the LMC, has a slightly more coherent [Mg/Fe]–[Fe/H] abundance pattern than the LMC at -2.0 < [Fe/H] < -1.0 (see, e.g., Figure 2). We infer separate sets of abundance vectors for using each high-Ia sample combined with the same low-Ia sample.

Because of small systematic differences in chemical abundances with stellar parameters, the APOGEE abundances have had zero-point shifts applied to them to force stars at solar metallicity near the Sun to have solar abundances (see, e.g., H. Jönsson et al. 2020). However, these offsets were applied to stars with generally hotter effective temperatures than our

sample here. Therefore, for each chemical element, we apply a new zero-point offset to force stars at solar [Mg/H] to have solar [X/Mg] abundances. These offsets are generally small (<0.05 dex), and are listed in Table 1. Applying these offsets allows for a more direct comparison with D. H. Weinberg et al. (2022). We then solve the two-process equations to return the  $q_{\rm cc}$  and  $q_{\rm Ia}$  abundance vectors. As discussed in D. H. Weinberg et al. (2022), these offsets have a small effect on the inferred abundance vectors, but have no effect on the residuals.

Before showing the abundance vectors, we first show in Figure 4 the ratio of the delayed to prompt process for each star in each galaxy, as given by

$$A_{\rm Ia}/A_{\rm cc} = \frac{10^{\rm [Fe/Mg]} - 10^{\rm [Fe/Mg]_{pl}}}{1 - 10^{\rm [Fe/Mg]_{pl}}}.$$

This is inferred directly from the [Fe/Mg] of a star, assuming that the pure CCSNe-only [Fe/Mg] abundance along the low-Ia/high- $\alpha$  "plateau" ([Fe/Mg]<sub>pl</sub>, shown as the black dashed

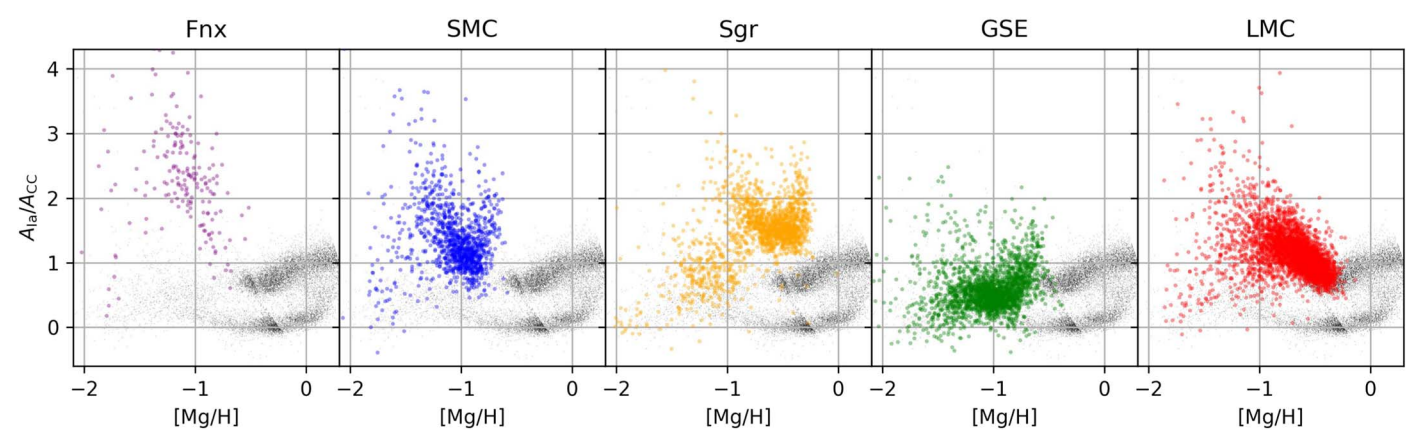


Figure 4. Ratios of the two-process amplitudes,  $A_{\rm Ia}/A_{\rm CC}$ , for each galaxy plotted as a function of metallicity ([Mg/H]). The MW sample is plotted in black and reproduced in each panel for comparison. Solar abundances correspond to  $A_{\rm Ia}=A_{\rm cc}=1$ , so stars with an  $A_{\rm Ia}/A_{\rm cc}$  ratio >1 have enhanced relative contribution from the "delayed" process, which we attribute to SNe Ia.

Table 1 Zero-point Offsets

[X/Mg]	Offset (dex)
Si	-0.020
S	0.002
Ca	0.006
C+N	-0.013
Na	-0.003
Al	-0.024
K	0.001
Cr	-0.015
Ni	-0.021
V	-0.017
Mn	-0.008
Co	0.003
Ce	-0.004

horizontal line in Figure 3) is -0.3, as done in D. H. Weinberg et al. (2019). This  $A_{\rm Ia}/A_{\rm cc}$  ratio plotted as a function of metallicity is useful to understand which process is contributing most significantly to the abundance of an element at a given point of a galaxy's evolution, providing insight into the general SFH of a galaxy. Unlike D. H. Weinberg et al. (2022) and T. Sit et al. (2024), but like D. H. Weinberg et al. (2019), we infer this ratio directly from the [Fe/Mg] values alone rather than the iterative multielement fit. We similarly infer the amplitude  $A_{\rm cc}$  directly from [Mg/H] using  $A_{\rm cc} = 10^{[{\rm Mg/H}]}$ , which assumes Mg to arise purely from the prompt (CCSNe) process and normalizes to  $A_{\rm cc} = 1$  at solar [Mg/H].

As shown in the left panel of Figure 4, Fornax (Fnx) stars generally have higher  $A_{\rm Ia}/A_{\rm cc}$  ratios than the stars in the other four satellite galaxies, indicating that this galaxy has had the largest relative contribution of the delayed process to its evolution. GSE exhibits a relatively simple  $A_{\rm Ia}/A_{\rm cc}$ -[Mg/H] pattern, with a low  $A_{\rm Ia}/A_{\rm cc}$  ratio that stays relatively flat at low metallicity, during which GSE formed stars from primarily gas polluted by the prompt core-collapse process alone. At [Mg/H] > -0.8, the  $A_{\rm Ia}/A_{\rm cc}$  increases as SNe Ia begins to contribute to the evolution of GSE. Sgr, SMC, and LMC all show a similar initial increase of the  $A_{\rm Ia}/A_{\rm cc}$  ratio with

increasing metallicity at low metallicity followed by a rapid decrease at higher metallicity, which can be interpreted as a later burst of star formation (see also B. Hendricks et al. 2014; D. L. Nidever et al. 2020; S. Hasselquist et al. 2021). The SMC and Sgr then show a final increase in  $A_{\rm Ia}/A_{\rm cc}$  ratio at the highest metallicities as the starbursts decline and SNe Ia begin to contribute anew to the chemical evolution of these galaxies. Only the LMC and Sgr overlap significantly with the high-Ia MW sample. At these metallicities, the LMC stars have about the same  $A_{\rm Ia}/A_{\rm cc}$  ratio as the MW stars, whereas the Sgr stars are about a factor of 2 higher.

#### 4. Abundance Vectors of the Two-process Model

Using the samples described in Section 2 and shown in Figure 3, we derive two sets of abundance vectors. For display purposes and to assist in the discussion, we group the elements into three groups:

- 1.  $\alpha$ -elements: O, Si, S, and Ca (Figure 5).
- 2. Odd-Z elements: C+N, Na, Al, and K (Figure 6).
- 3. Fe-peak<sup>+</sup>: Cr, Ni, V, Mn, Co, and Ce (Figure 7). 10

The elemental abundances of each sample are shown in the left panels of Figures 5–7 and the inferred two-process abundance vectors are shown in the middle panels. We also show in the right panels the  $f_{\rm cc}$  values for each element along each sample, defined as

$$\mathrm{f_{cc}} = rac{A_{\mathrm{cc}}q_{\mathrm{cc}}}{A_{\mathrm{cc}}q_{\mathrm{cc}} + A_{\mathrm{Ia}}q_{\mathrm{Ia}}}.$$

This  $f_{\rm cc}$  value indicates how much of some element comes from the prompt (assumed to be core-collapse) enrichment mechanism, and can therefore be a useful tool in understanding the dominant enrichment mechanism at a given metallicity for each stellar sample.  $f_{\rm cc} \simeq 1$  indicates that element is being produced entirely in CCSNe and  $f_{\rm cc} < 0.5$  indicates the delayed mechanism (e.g., SNe Ia) is the dominant enrichment

C is not an odd-Z element, but due to stellar evolution effects, we cannot consider C and N separately as their surface abundances are affected by mixing mechanisms in red giant branch stars (M. Salaris et al. 2015). We instead consider the number-weighted sum of C and N abundances, as the sum of these elements after mixing events should be similar to the birth C+N abundance

<sup>&</sup>lt;sup>10</sup> Ce is commonly considered an s-process element and is synthesized in large quantities by AGB stars, but we include the heaviest elements here for presentation purposes.

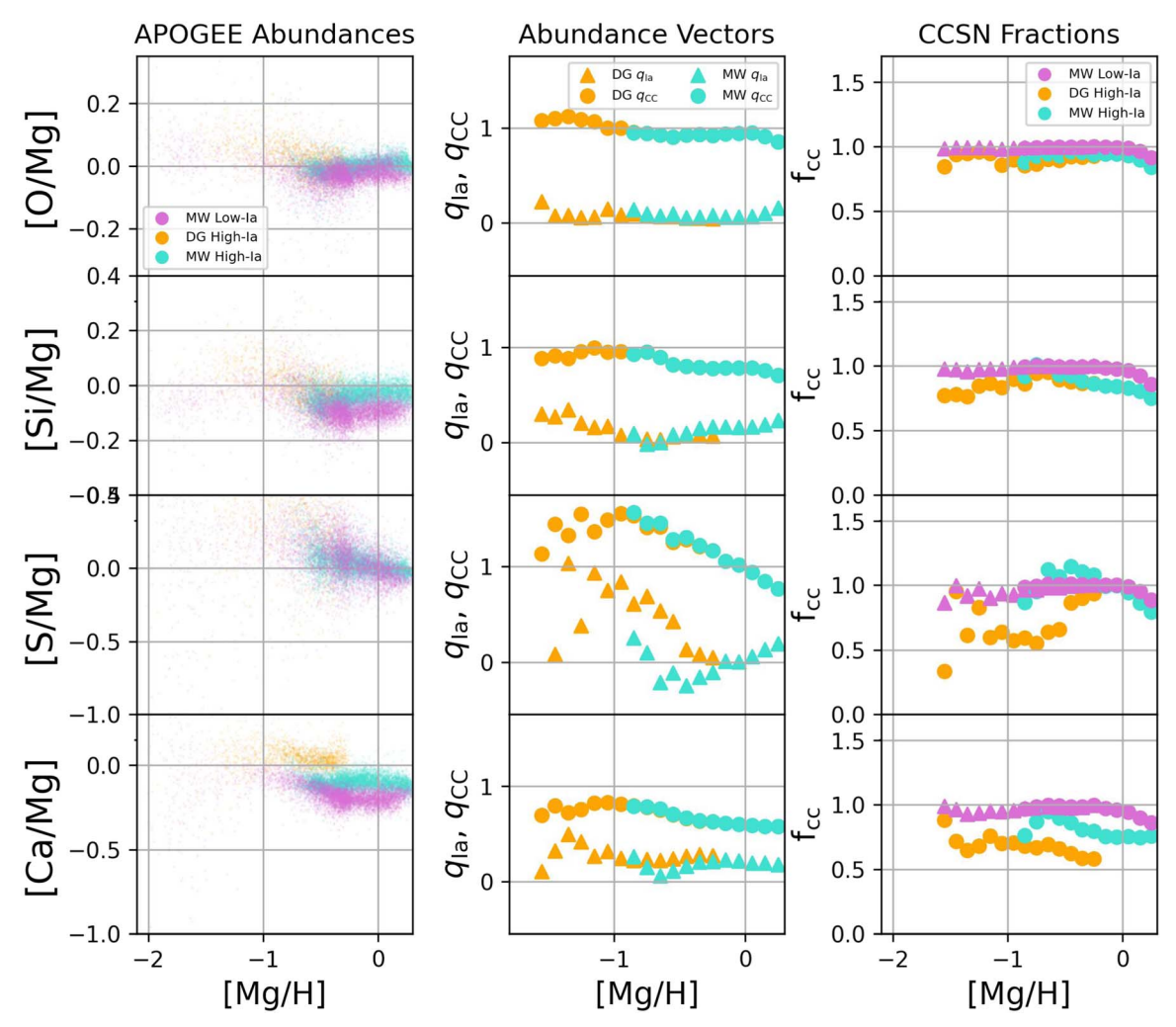


Figure 5. Left column: APOGEE  $\alpha$ -element abundances for the high-Ia DG (orange), high-Ia MW (turquoise), and low-Ia (orchid) samples used to derive the parameters of the two-process model. Middle column: the abundance vectors for each element in orange (fit to high-Ia DG sample) and turquoise (fit to high-Ia MW sample). Right column: the  $f_{cc}$  value for each sample, which indicates the fraction of the element that comes from the prompt CCSNe component at that metallicity for stars along the median low-Ia or high-Ia track of the MW or the median high-Ia track of the DG sample.

mechanism. Note that even if an element has a large IMF-averaged SNe Ia yield as indicated by the  $q_{\rm Ia}$  vector (e.g., Ni, with  $q_{\rm Ia}\approx 0.5$ ),  $f_{\rm cc}\approx 1$  for low-Ia stars (orchid points in Figures 5–7) because these stars are inferred to have nearly pure CCSNe enrichment based on their [Fe/Mg] abundances. Additionally, because the  $f_{\rm cc}$  value depends on the abundance vectors, they can be different for the high-Ia DG sample and the high-Ia MW sample, as we infer different abundance vectors for these samples for some elements (e.g., Ca, C+N, Al, Ni, and Ce, described in more detail below). We find that the abundance vectors we infer from the high-Ia MW sample are nearly the same as those inferred by D. H. Weinberg et al. (2022), despite the slightly lower  $T_{\rm eff}$  and  $\log g$  distribution of our high-Ia MW sample.

In the following section, we use these two sets of abundance vectors to predict the elemental abundances of each galaxy, focusing on what the residuals might mean for galaxy evolution or breakdowns in the two-process model assumptions. However, the fact that we even derive different abundance vectors for some elements between the high-Ia MW sample and the high-Ia DG sample (Sgr) suggests we should expect large residuals when using the high-Ia MW sample to predict the abundances of the various satellite galaxies. In the context of

the two-process model, different abundance vectors mean that the IMF-averaged yields of that process are different between the MW and Sgr. For elements like C+N (top row of Figure 6) or Ce (bottom row of Figure 7), the differences in the inferred  $q_{\rm Ia}$  vectors could be related to an increased contribution of AGB stars to the delayed process in Sgr. The causes for differences in the inferred  $q_{\rm Ia}$  vectors for elements like Ni and Co (Figure 7) are less obvious. The small difference in  $q_{\rm Ia}$ vectors for Ca (Figure 5) results in large changes in inferred  $f_{cc}$ values, suggesting the delayed process contributed at a much larger fraction to the Ca in Sgr than it did in the MW (if the model assumptions are correct). Finally, we actually infer negative  $q_{\rm Ia}$  vectors for Al, leading to nonphysical values for  $f_{\rm cc}$  $(f_{\rm cc} > 1)$ , suggesting there is likely some issue with the twoprocess model assumptions for this element. We explore potential causes for these differences of inferred  $q_{Ia}$  in Section 6, but first we analyze how well each model can predict the abundances of stars across all galaxies.

# 5. Residual Abundance Analysis Results

We use the derived abundance vectors shown in the middle panels of Figures 5–7 to predict the abundances of satellite galaxy stars. Because the high-Ia samples differ in metallicity

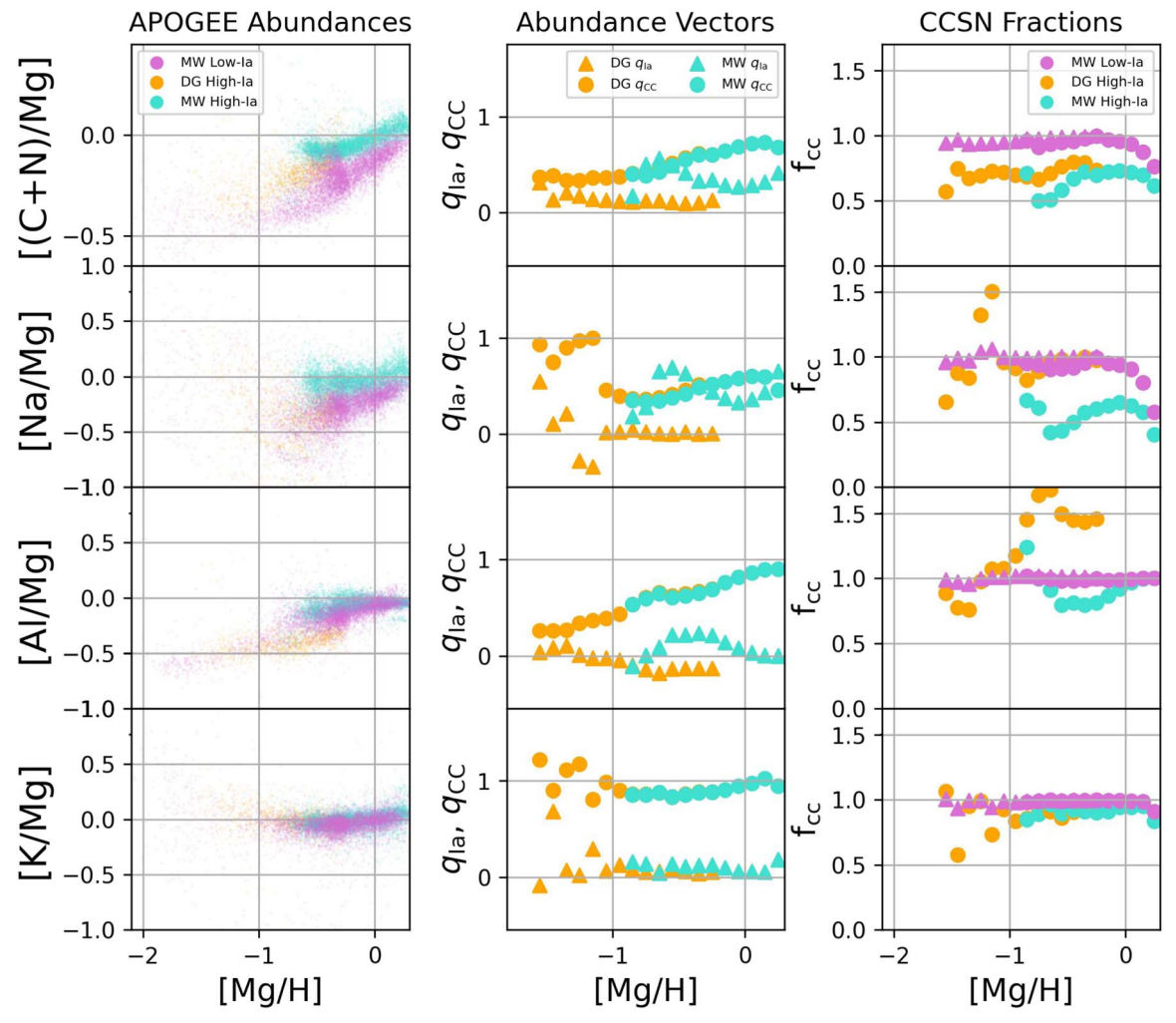


Figure 6. Same as Figure 5, but for the odd-Z elements.

coverage, the MW two-process model is limited to predicting the abundances of the most metal-rich stars in the satellite galaxies, whereas the DG two-process model is able to predict abundances for most of the metallicity range spanned by each satellite galaxy. In Figure 8, we show the median abundance residuals (observed/predicted from the two-process model) across all stars able to be predicted by each model for the vectors derived from the MW stars (top panel) and DG (Sgr) sample (bottom panel). The boxes indicate the  $\pm 1\sigma_{\rm MAD}$  (a robust measurement of the standard deviation using astropy. stats.mad\_std,  $\sigma_{MAD} \simeq 1.48^*$ Median Absolute Deviation) of the distribution from which the median is taken. The residuals of the satellite galaxies are much larger when the MW twoprocess model is used to predict the abundances than when the DG two-process model is used. Specifically, we find that when using the MW model to predict satellite galaxy abundances:

- The abundance of Ce is underpredicted by 0.2 dex for Sgr and the LMC, but not for GSE.
- 2. The abundances of C+N, Na, Al, Ni, Mn, and Co are overpredicted by the model by 0.1–0.3 dex, with the largest overpredictions found for Sgr and the LMC.
- 3. The abundance of Ca is underpredicted by 0.1 dex for Sgr, LMC, and GSE, which is significant given the small scatter for each galaxy.

- 4. The abundances of O, Si, K, and Cr are all close to the model predictions.
- 5. S and V are the least well-measured abundances in our sample (as indicated by the large boxes that indicate scatter in the residuals in Figure 8), but the satellite galaxies show large residuals in both elements, with GSE showing the smallest residuals.

These residual abundance patterns are broadly consistent with what has been found in D. H. Weinberg et al. (2022) for a smaller sample of LMC stars and T. Sit et al. (2024) for the LMC and Sgr, the latter study carefully correcting for small systematic abundance differences as a function of  $\log g$ . In the context of the two-process model, elements that are overpredicted by the model (negative values of observed/predicted abundances in the top panel Figure 8; e.g., C+N, Al, and Ni) mean that one or both of the processes are not producing enough of that element in a given galaxy given its stellar [Fe/Mg]-[Mg/H] abundances. We explore potential reasons for this throughout Section 6. Conversely, elements that are underpredicted by the model (positive values of observed/predicted abundances in the top panel of Figure 8; e.g., Ce) mean that one or both of the processes are producing more of this element than is expected given the stellar [Fe/Mg]-[Mg/H] abundances, or that there is a separate process that is producing this element that is not active in the stellar sample used to fit the model parameters. In Section 6.1, we

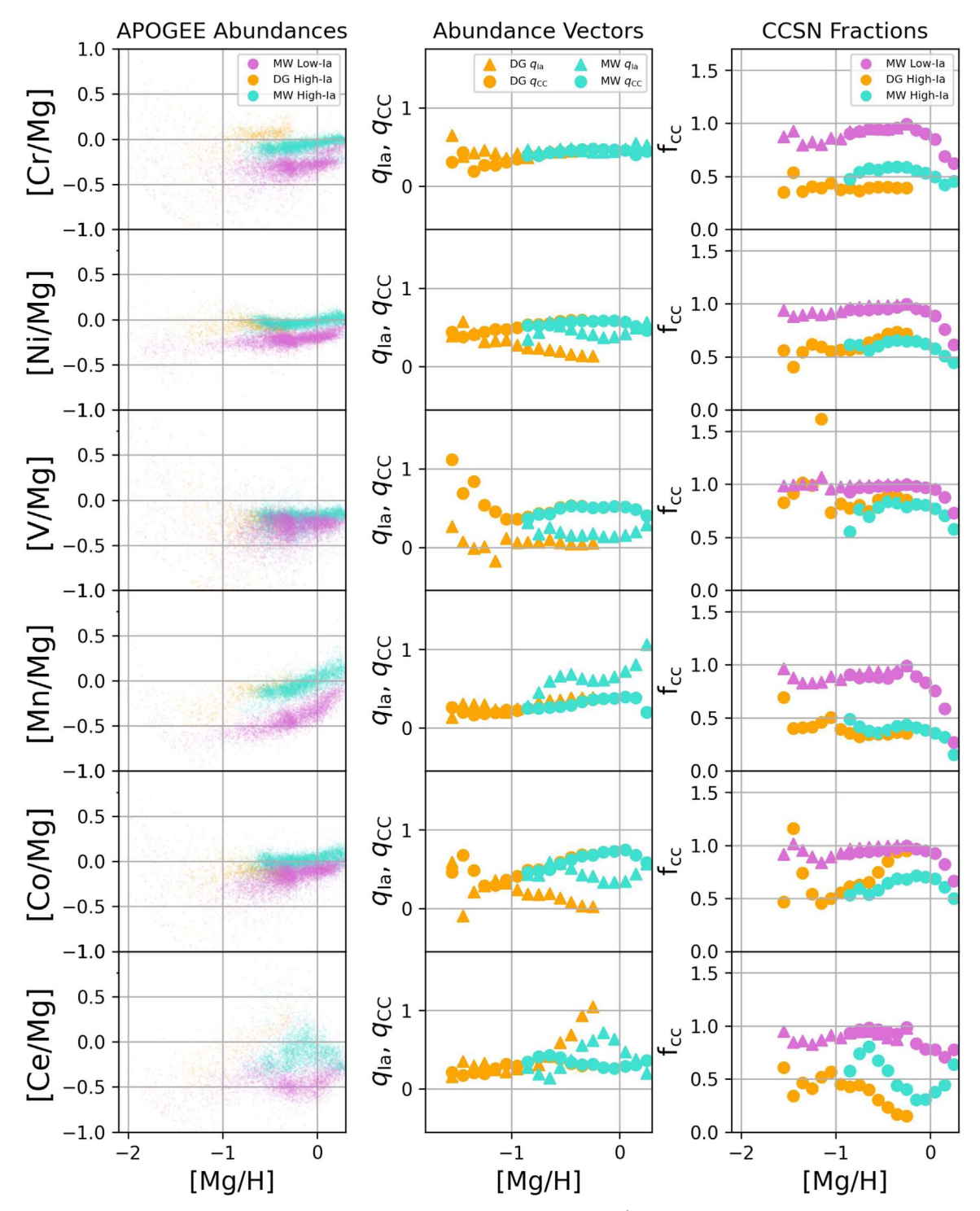


Figure 7. Same as Figure 5, but for the Fe-peak<sup>+</sup> elements.

argue that the underprediction of Ce in the satellite galaxies is due to an increased contribution from AGB stars.

Despite the large residuals when using the MW two-process model to predict the abundances of the satellite galaxies, the bottom panel of Figure 8 shows that when using the DG two-process model to predict the abundances of the satellite galaxies, the residuals are very close to zero for all galaxies, with differences up to 0.1 dex in a few cases. Therefore, the  $q_{\rm cc}$  and  $q_{\rm Ia}$  vectors that were fit to the DG sample changed in such a

way relative to what they were when fit to the MW sample to accurately predict the abundances of the satellite galaxy stars. Specifically, the  $q_{\rm Ia}$  vectors of C+N, Na, Al, Ni, V, and Co all decreased, whereas the  $q_{\rm Ia}$  vectors of Ca and Ce increased, as seen by comparing the orange triangles to the turquoise triangles in the middle panels of Figures 5–7. The changes in abundance vectors were able to accurately predict the satellite galaxy abundances despite the wide range in  $A_{\rm Ia}/A_{\rm cc}$  ratios (Figure 4).

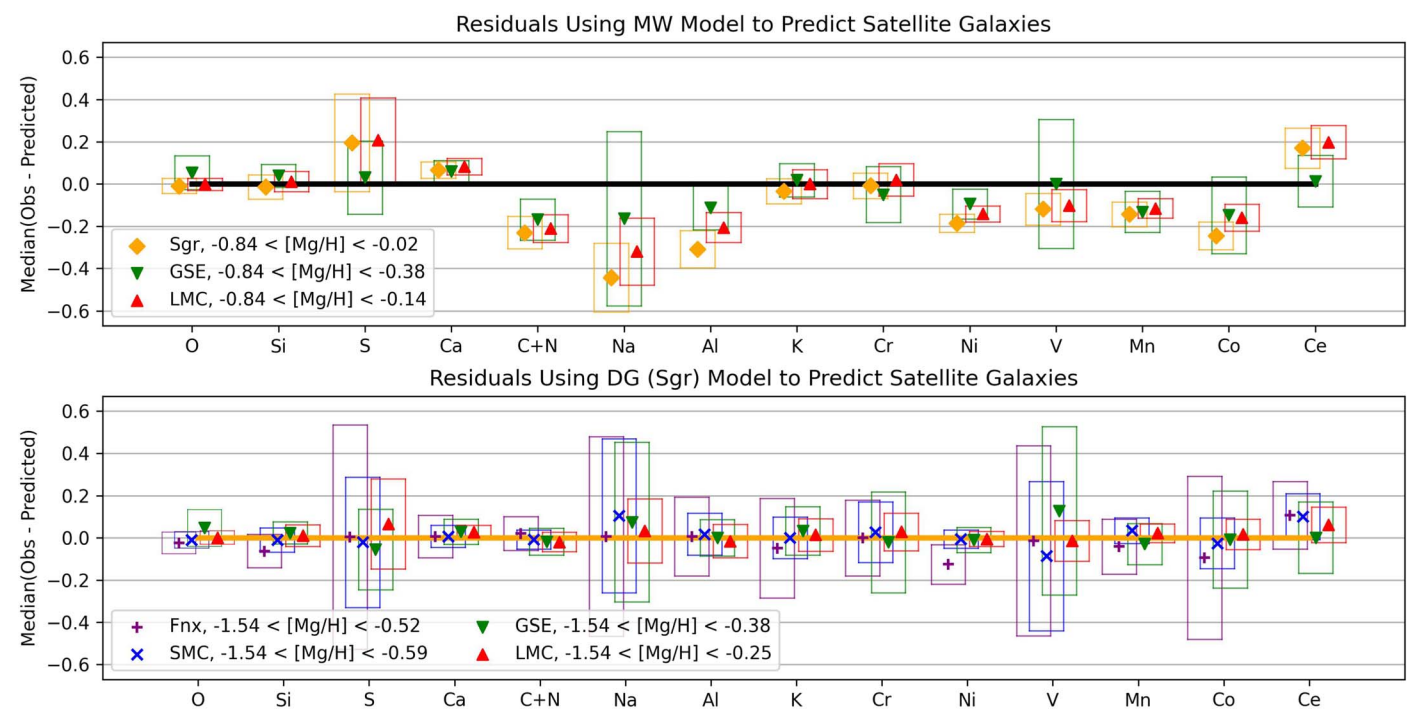


Figure 8. Median abundance residuals (observed/model prediction) for the satellite galaxy stars predicted using the two-process model fit to MW stars (top panel) and for the satellite galaxy stars predicted using the two-process model fit to the DG (Sgr) stars (bottom panel). The thick solid lines indicate where the residuals are zero, by construction, for each galaxy used to predict the model. The legends in the upper right indicate the metallicity range over which the residuals were calculated. The thinner solid lines around each point indicate the  $\pm 1\sigma_{\rm MAD}$  (a robust measurement of the standard deviation using astropy.stats.mad\_std,  $\sigma_{\rm MAD} \simeq 1.48^*$  median absolute deviation) of the distribution from which the median is taken, colored by galaxy, as indicated in the legend.

The difference between the two panels of Figure 8 is the principal result of this paper. In the range of overlapping metallicity, the APOGEE abundances of satellite galaxy stars are significantly different from those of the MW disk stars matched in [Mg/H] and [Mg/Fe], an effect seen for more than half of the elements examined here. However, once matched in [Mg/H] and [Mg/Fe], the abundances of these five satellite galaxies are quite similar to each other.

#### 6. Discussion

The small residuals between observed and predicted abundances of the satellite galaxies when using the DG two-process model suggest that the two-process model is still a viable description of how chemical enrichment is occurring in the satellite galaxies, i.e., the amount of enrichment from the prompt source, [Mg/H], combined with the ratio of delayed-to-prompt enrichment ([Fe/Mg]), allows for accurate predictions of the abundances of all of the other elements. In the following discussion, we attempt to explain why there are large residuals for the satellite galaxies when using the MW two-process model, linking the differences to potential differences in the enrichment processes or breakdowns in the model assumptions. We consider the following:

- 1. The delayed process, represented by the  $q_{\rm Ia}$  abundance vector, is likely the sum of both SNe Ia ejecta and AGB ejecta, the latter of which likely contributes at a larger relative amount to the satellite galaxies than in the MW. This could explain the Ce underpredictions in the satellite galaxies using the MW two-process model, and some of the C+N residual patterns (Section 6.1).
- 2. The abundance vectors for the two-process model are derived in bins of size 0.1 dex in [Mg/H], and thus any

- metallicity-dependent production of the elements is assumed to depend on Mg abundance. It is therefore possible that the model is not capturing the full intricacies of the metallicity-dependent production of some elements in one or both of the processes. For example, we find some evidence that the production of some of the metallicity-dependent elements, e.g., Al, is more dependent on C+N, suggesting that the Mg assumption might be responsible for some of the residuals in the satellite galaxies when using the MW two-process model to predict their abundances (Section 6.2).
- 3. For an element with a metallicity-dependent yield, large inflows of pristine gas can drive departures from the two-process model by reducing [Mg/H] without changing abundance ratios. A major dilution event could have affected the MW between the formation of the low-Ia and high-Ia sequences (e.g., C. Chiappini et al. 1997; E. Spitoni et al. 2019). This scenario could explain why most of the metallicity-dependent elements show large residuals in the satellite galaxies and the metallicity-independent elements do not (Section 6.3).
- 4. The IMF and/or nature of the outflows may have been fundamentally different between the satellite galaxies and the MW, with the satellite galaxies preferentially losing some elements as compared to the MW. This plausibly explains elements with negative abundance vectors, e.g., Al and Na, as shown in the middle panel of Figure 6 (Section 6.4).
- 5. The satellite galaxies may have had a larger fraction of atypical SNe, e.g., sub-Chandrasekhar-mass SNe Ia, to give rise to the larger residuals in Ca, Ni, Mn, and Co, all elements with increased contribution from the delayed process in the MW (Section 6.5).

The scenarios mentioned above and discussed in more detail below apply to the metal-rich (-0.9 < [Mg/H] < 0.00) stars of the LMC, Sgr, and GSE. However, any explanation or combination of explanations must account for the MW two-process model residual patterns of these satellite galaxies as well as the fact that the DG two-process model applied to the satellite galaxies results in little to no residuals for all elements across all satellite galaxies.

#### 6.1. The Effects of AGB Stars

The two-process model assumes that the elements are produced in some combination of a prompt and a delayed mechanism, which is typically attributed to CCSNe and SNe Ia, respectively. However, AGB stars also contribute to the chemical enrichment of a galaxy, producing a significant fraction of the C and N in MW disk stars (e.g., C. Kobayashi et al. 2020a) and the majority of the Ce (e.g., N. Prantzos et al. 2020). In principle, the contribution of AGB stars would be included in the two-process abundance vector of the delayed enrichment mechanism,  $q_{\rm Ia}$ . However, if the ratio of AGB enrichment to SNe Ia enrichment is lower for the MW than it is for the DGs, then we would expect the satellite galaxies to have underpredicted abundances from the MW two-process model for these elements.

The top panel of Figure 8 shows that the metal-rich Sgr and LMC stars have their Ce abundances underpredicted by 0.2 dex. The underprediction is not seen in the GSE stars, plausibly because these stars have lower  $A_{\rm Ia}/A_{\rm cc}$  ratios than Sgr and the LMC, over most of this metallicity range (see Figure 4). Ideally, one could develop a three-process model to separate the AGB enhancement, but calibrating such a model requires at least one additional element with a known ratio of AGB/SN Ia/CCSN enrichment (see, e.g., E. J. Griffith et al. 2022). Still, *s*-process enhancement has been measured in these galaxies before (e.g., A. McWilliam et al. 2013), and the underprediction of Ce by the MW two-process model is very likely a result of not properly taking into account a third AGB process.

If the model underpredictions of [Ce/Mg] in the satellite galaxies at [Mg/H] > -0.8 are due to a delayed process that has more AGB contribution than the delayed process in the MW, then we might also expect residual trends in [C/Mg] and [N/Mg] (which we show together as [(C+N)/Mg] to negate the effects of internal stellar mixing) to be correlated with [Ce/Mg], as these elements are also produced in nonnegligible quantities in AGB stars (C. Kobayashi et al. 2020a). In the top row of Figure 9, we first show the residual [(C+N)/Mg] abundances as a function of [Mg/H] for both Sgr (left) and the LMC (right). We see that both galaxies, aside from the most metal-poor stars, exhibit a residual [(C+N)/Mg] abundance that gets closer to zero with increasing [Mg/H]. The abundances of the most metal-rich stars are still overpredicted by  $\sim 0.15$  dex, suggesting that there are likely additional reasons beyond AGB enrichment to explain the [(C+N)/Mg] residuals.

Still, we can assess the extent to which AGB production might be influencing the C+N abundances of these galaxies by analyzing how the residuals change as a function of "excess" [Ce/Mg] abundance, which we notate as  $\Theta_{\rm [Ce/Mg]}$ . This quantity is defined as the difference between a star's [Ce/Mg] abundance and the abundance of the median high-Ia MW sample at that same metallicity, demonstrated in the

middle panels of Figure 9. Assuming that Ce is produced entirely in AGB stars at these metallicities, we use this as a measurement of excess AGB contribution in a star as compared to a "typical" star in the MW high-Ia sequence.

The bottom panel of Figure 9 shows that  $\Theta_{\text{[Ce/Mg]}}$  is correlated with the residual [(C+N)/Mg] abundance for Sgr, but not so for the LMC. So, for Sgr, the smaller C+N residuals at higher [Mg/H] are plausibly due to the fact that AGB stars begin to create C and N in large quantities, "making up" for whatever process failed to produce the expected amount of C+N from the MW two-process model. This is apparently not the case for the LMC, but this might be expected given that the LMC has a much lower  $A_{Ia}/A_{cc}$  ratio at these metallicities than Sgr (see Figure 4). If AGB stars play a larger role in enriching the satellite galaxies than in the MW, we would expect to see the largest differences at metallicities where the delayed process dominates. However, AGB enrichment cannot explain why the C+N residual decreases with increasing [Mg/H] for the LMC, nor why these galaxies have such large residuals to begin with.

In general, the [Ce/Mg] residuals of the satellite galaxies for the DG two-process model are much smaller, as shown in the lower panel of Figure 8. The SMC and Fnx have [Ce/Mg] residuals of  $\sim$ 0.1 dex, suggesting that these two galaxies have had the largest amount of AGB contribution to their chemical evolution.

### 6.2. Metallicity Dependence

In addition to overpredicting [(C+N)/Mg], the MW twoprocess model also overpredicts the abundances of [Al/Mg] and [Na/Mg] (see top panel of Figure 8). Aside from the aforementioned contributions of AGB stars to C+N, these elements are largely produced by the prompt process, and in such a way that depends on metallicity, as demonstrated by their abundance vectors shown in the middle panel of Figure 6. One potential reason for these overpredictions could be that, while traditionally [Fe/H] has been used as a tracer for overall metal abundance (metallicity), the two-process model uses [Mg/H] because it serves as a tracer for overall enrichment from the prompt process only (with the assumption that Mg is produced in the prompt process only). However, the detailed nucleosynthetic processes that actually create a specific element might be more dependent on other elements, such as C, N, and/or O, in the case of producing Na and Al via hydrostatic carbon and neon burning (see, e.g., J. W. Truran & W. D. Arnett 1971). Therefore, we might expect smaller Al and Na residuals if we use C+N as a reference element rather than Mg.

Unfortunately, it is not trivial to swap in C+N for Mg and rederive the two-process model parameters using C+N as the reference element, as C+N is created in both processes. Instead, similar to what was done in Figure 9, we first look at whether or not the residual Al abundances are correlated with C+N abundance, which might indicate that the production of Al depends on the abundance of C+N. The top panel of Figure 10 shows [Al/Mg] residuals as a function of [Mg/H] again for Sgr (left) and the LMC (right). Sgr shows essentially flat residuals across all metallicity, whereas the LMC shows residuals that get slightly closer to 0 with increasing [Mg/H], indicating that the more metal-rich stars in the LMC have [Al/Mg] abundances that are closer to the model predictions. The second row of Figure 10 introduces  $\Theta_{[(C+N)/Mg]}$ , which is the difference between a star's [(C+N)/Mg] abundance and that of

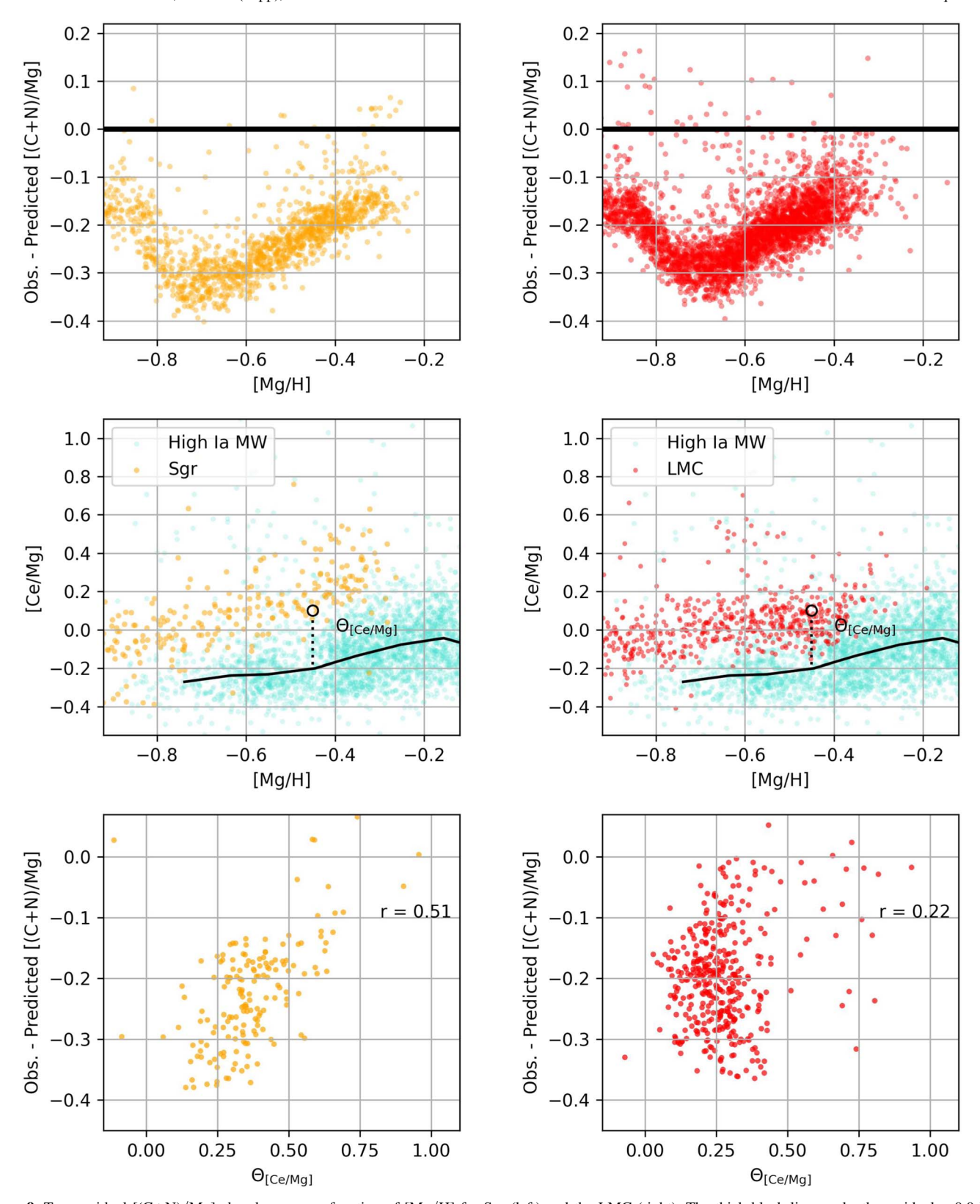


Figure 9. Top: residual [(C+N)/Mg] abundances as a function of [Mg/H] for Sgr (left) and the LMC (right). The thick black line marks the residual = 0.0 line. Middle: [Ce/Mg] abundance plotted as a function of [Mg/H] to demonstrate that the parameter  $\Theta_{[Ce/Mg]}$  is the excess [Ce/Mg] abundance of a satellite galaxy star above that of the MW median trend (black line). The high-Ia MW sample is reproduced in each panel as turquoise points. Bottom: the residual [(C+N)/Mg] abundance plotted as a function of excess [Ce/Mg],  $\Theta_{[Ce/Mg]}$ . Pearson correlation coefficients are indicated in the bottom panels.

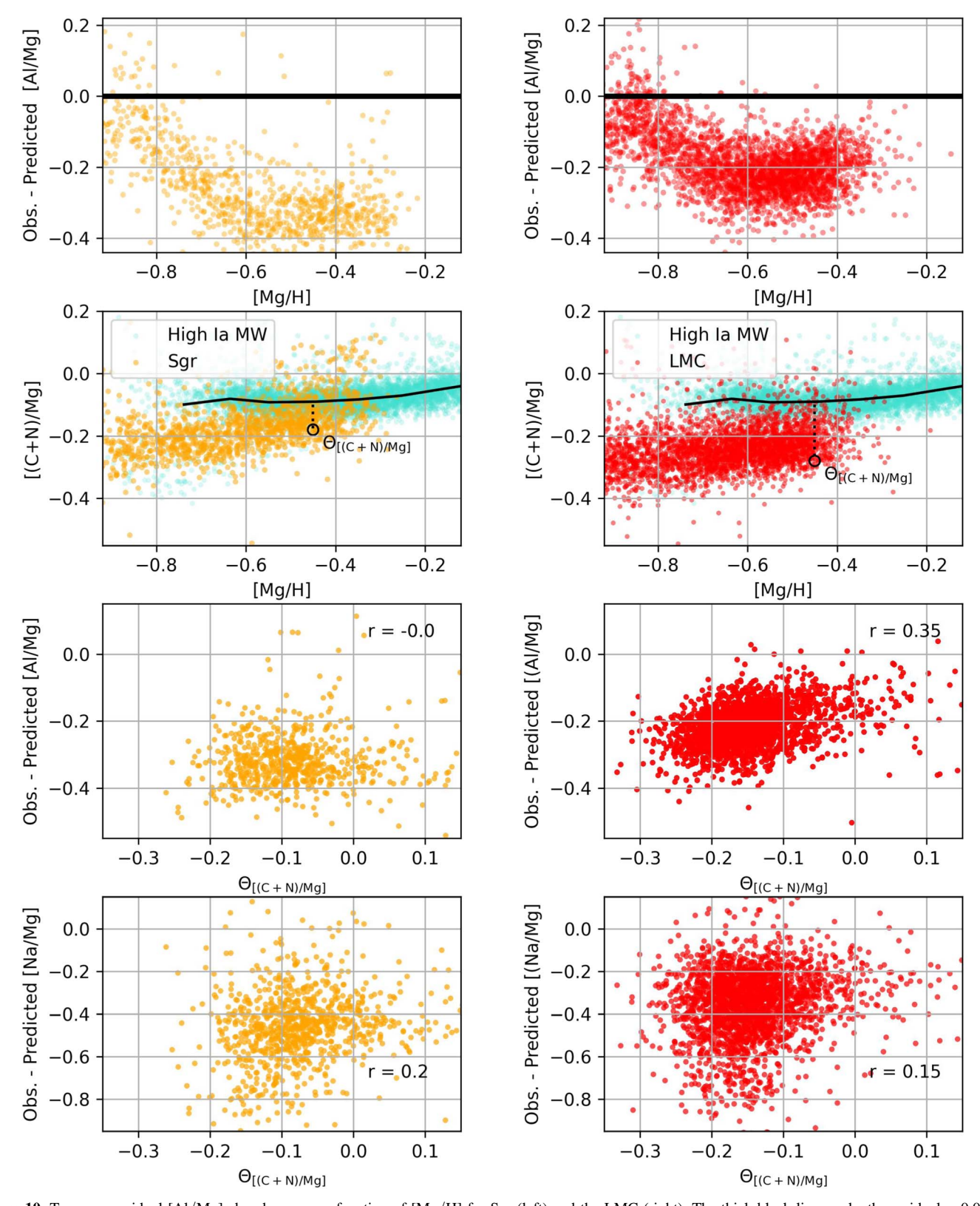


Figure 10. Top row: residual [Al/Mg] abundances as a function of [Mg/H] for Sgr (left) and the LMC (right). The thick black line marks the residual = 0.0 line. Second row: [(C+N)/Mg] abundance plotted as a function of [Mg/H] to demonstrate that the parameter  $\Theta_{[(C+N)/Mg]}$  is the excess [(C+N)/Mg] abundance of a satellite galaxy star above that of the MW median trend (black line). The high-Ia MW sample is reproduced in each panel as turquoise points. Third row: the residual [Al/Mg] abundance plotted as a function of  $\Theta_{[(C+N)/Mg]}$ . Fourth row: the residual [Na/Mg] abundance plotted as a function of  $\Theta_{[(C+N)/Mg]}$ . Pearson correlation coefficients are indicated in the bottom two rows.

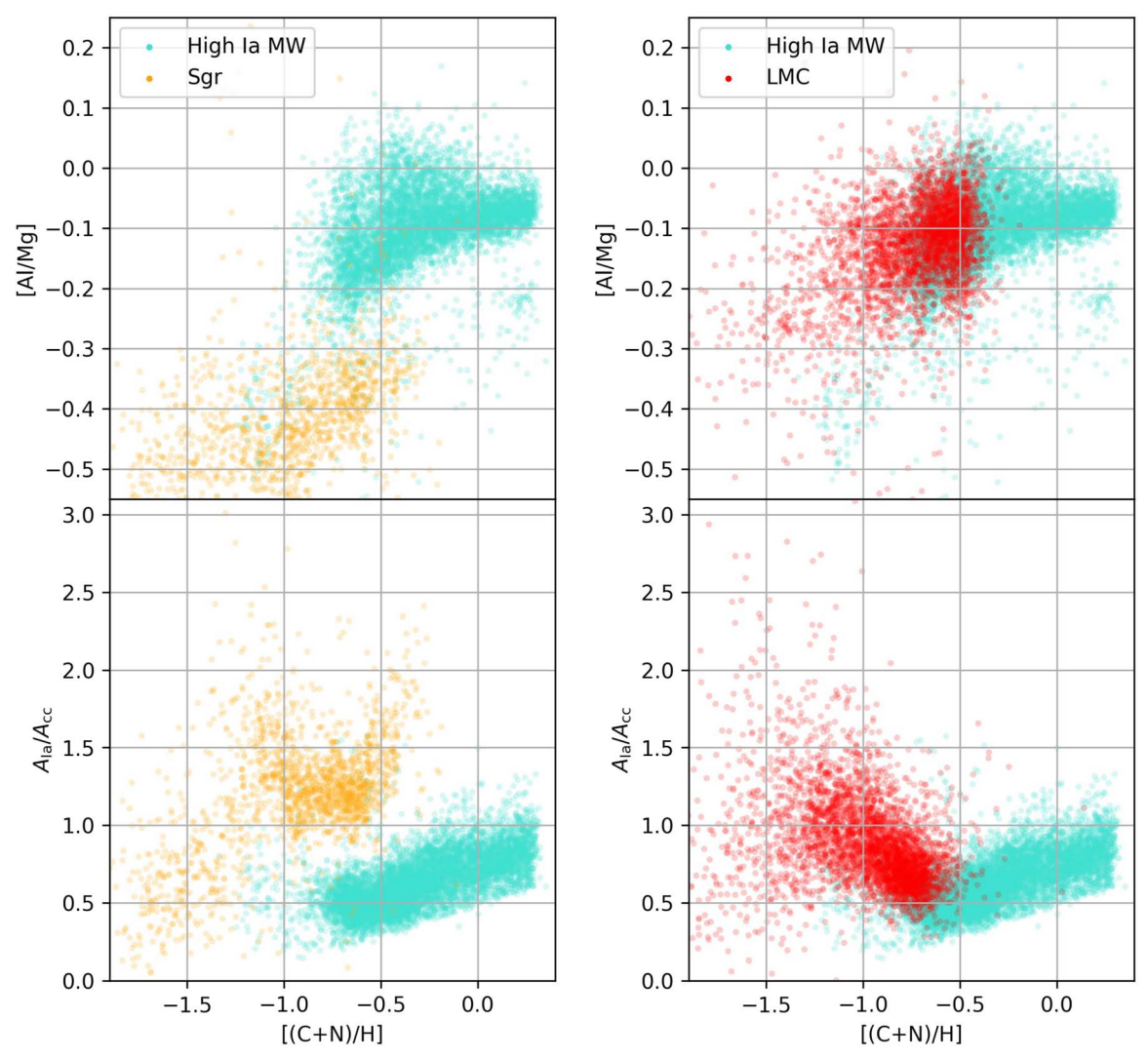


Figure 11. Top: [Al/Mg] vs. [(C+N)/H] for Sgr (left, orange) and the LMC (right, red), with the MW high-Ia sample reproduced in each panel as the turquoise points. Bottom:  $A_{Ia}/A_{CC}$  ratios as a function of [(C+N)/H].

the median high-Ia MW trend. This is similar to  $\Theta_{\rm [Ce/Mg]}$ , described in Section 6.1, but for this element the satellite galaxies are deficient relative to the MW at fixed [Mg/H] instead of enhanced. The third row shows that this quantity is uncorrelated with [Al/Mg] abundance residuals for Sgr, but correlated with the LMC. We do not see any correlations for Na, which might be because the Na abundances at these metallicities are too high.

Thus, from the third row of Figure 10, we again have a situation where one satellite galaxy exhibits a correlation and the other does not. However, we argued in Section 6.1 that Sgr, with its higher  $A_{\rm Ia}/A_{\rm CC}$  ratios and correlations between  $\Theta_{\rm [Ce/Mg]}$  and residual [(C+N)/Mg], exhibits a significant contribution from AGB stars to its C+N abundance at these metallicities. The LMC, on the other hand, seems to have C+N coming almost entirely from the prompt process at these metallicities. If the production of Al in the prompt process is more dependent on C+N than it is on Mg, as theoretically expected, then we would expect the LMC to have more high-Ia MW-like [Al/Mg] abundances at fixed [(C+N)/H] abundance. This is exactly what we find in the upper-right panel of Figure 11. For the LMC stars, there is substantial overlap in [Al/Mg] with the MW high-Ia sample at fixed [(C+N)/H].

Sgr, shown in the upper-left panel of Figure 11, is still deficient, but that is plausible because the C+N is coming from AGB for Sgr, whereas it is almost entirely coming from the prompt process in the LMC, as indicated by the  $A_{\rm Ia}/A_{\rm CC}$  ratios shown in the bottom panel of Figure 11.

This scenario does not quite explain why the [(C+N)/Mg] abundances of the satellite galaxies are low in the first place. However, it could explain why the DG two-process model finds slightly negative  $q_{Ia}$  vectors for Al and Na, as shown in the middle panel of Figure 6. Essentially the DG (Sgr) stars used to fit the model have a [Al/Mg] abundance that is lower than the MW low-Ia sample. At these metallicities, the [Al/Mg] abundance of the MW low-Ia sample represents the pure prompt abundance. To be below the pure prompt [Al/Mg] abundance means that the  $q_{\mathrm{Ia}}$  vector must work to remove Al from the galaxy, a description that is not necessarily physical. However, if a third process could be introduced to account for the increased [(C+N)/H] in Sgr due to AGB stars, one could, in principle, modify the two-process model such that the metallicity dependence of elements like Al is on [(C+N)/H]<sub>cc</sub> rather than [Mg/H]. Alternatively, we could fit the two-process model to the LMC stars instead, and use [(C+N)/H] as the reference element as Section 6.1 argues that the LMC has little

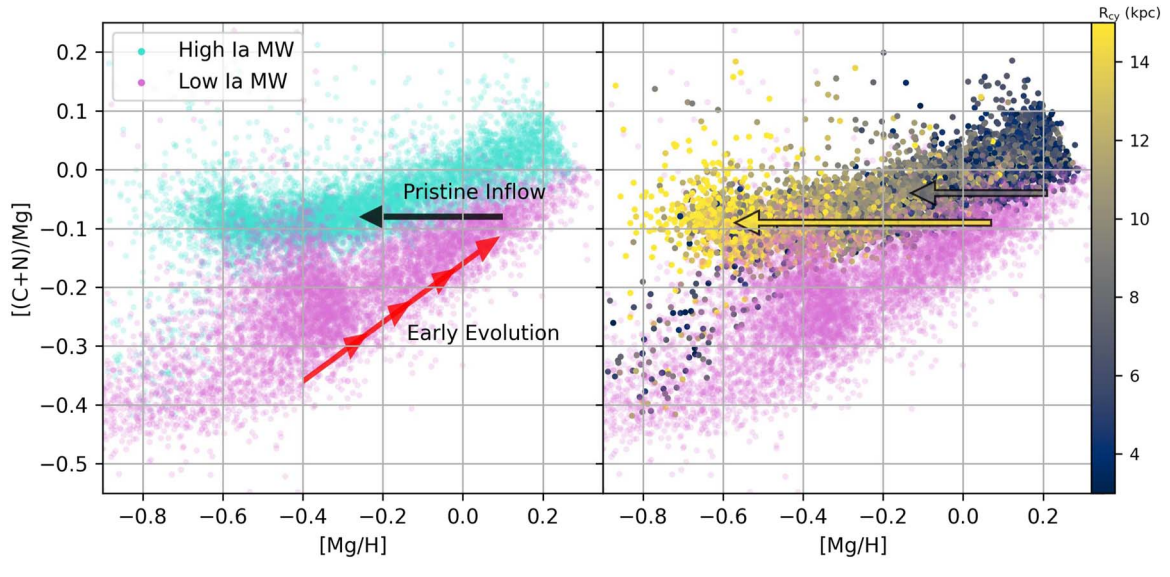


Figure 12. Left: [(C+N)/Mg]-[Mg/H] abundance patterns for the high-Ia MW sample (turquoise) and the low-Ia MW sample (orchid). The series of red arrows indicates the time evolution of the low-Ia MW sample. The black arrow indicates how the abundance of gas changes when pristine gas is added to the MW (overall metallicity drops, but relative abundance stays the same). Right: same as the left but now the high-Ia sample is colored by Galactic cylindrical radius ( $R_{cy}$ ). The arrows indicate that different regions of the MW potentially had more or less dilution before forming stars again.

AGB contribution to [(C+N)/H] at these metallicities. This is beyond the scope of this work, but we do emphasize that the upper-right panel of Figure 11, which shows the LMC stars overlapping with the high-Ia sample in [Al/Mg], is evidence for a stronger Al dependence on C+N than Mg in the prompt process.

# 6.3. Inflows

While the [Al/Mg] overlap for the LMC and high-Ia MW samples at fixed [(C+N)/H] suggests that the assumed metallicity dependence of the model is a plausible explanation for the Al abundance residuals as well as the decreasing [(C+N)/Mg] residuals with increasing [Mg/H] for the LMC, this explanation still does not account for why the [(C+N)/Mg] abundances of the satellite galaxies are lower than the predictions to begin with. One potential explanation is that the inflow of pristine gas was a much larger factor in the chemical evolution of the MW than it was for the satellite galaxies. As described in detail below, the inflow of pristine gas would lower the overall metallicity of a galaxy while keeping the [X/Mg] abundance ratios at whatever level they were at right before the pristine inflow. For the metallicitydependent elements, this would mean that stars formed immediately after the inflow would appear to have higher [X/Mg] ratios than their metallicity would suggest. This could lead to large residuals when using the MW two-process model to predict the abundances in other galaxies that did not have such an inflow event.

A wide range of MW Galactic archaeological work over the past decades has put together a picture that the MW low-Ia (high- $\alpha$ ) sequence formed first during a period of vigorous star formation, with the gas-forming stars enriching up to nearly solar metallicity before SNe Ia began to contribute to the evolution (e.g., B. M. Tinsley 1979). The high-Ia sequence, with its more solar-like  $\alpha$ -element abundances, formed some time after. Moreover, this high-Ia sequence is only a sequence if stars from all Galactic disk positions are considered at the same time, with the outer disk containing a higher fraction of

metal-poor stars and the inner disk containing a relatively higher fraction of metal-rich stars (e.g., M. R. Hayden et al. 2015; D. H. Weinberg et al. 2019). Age studies have revealed that, while each Galactic position contains a range of metallicities along the high-Ia sequence, the youngest stars become more metal-poor with increasing Galactic radius (e.g., J. T. Mackereth et al. 2017; S. Hasselquist et al. 2019). Therefore, we are now putting together a picture of our Galaxy that shows that the low-Ia sequence really is an evolutionary sequence, and formed first. Then, after an infall of pristine gas (perhaps even from the GSE merger, e.g., I. Ciuca et al. 2024) that diluted the now supersolar gas of the MW to some metallicity, with this dilution apparently stronger with increasing Galactic radius (qualitatively consistent with T. Buck et al. 2023 conclusions from simulations), stars began to form again at some point on the high-Ia sequence (C. Chiappini et al. 1997; E. Spitoni et al. 2019). Support for such a sudden infall was found by E. Spitoni et al. (2024), who found that their twoinfall model results in very few stars ( $\sim$ 1% of all stars formed) formed during this period of dilution. Radial migration then likely played a role in mixing high-Ia populations across the Galaxy (e.g., R. Schönrich & J. Binney 2009; M. R. Hayden et al. 2015; S. R. Loebman et al. 2016; S. Hasselquist et al. 2019; J. Lian et al. 2020), but what we care about in the twoprocess model is that the MW high-Ia stars likely formed from a combination of gas that was enriched to supersolar metallicity and pristine gas.

A schematic of this scenario is shown in Figure 12, where we show the [(C+N)/Mg]-[Mg/H] abundance plane for just the two MW samples. C+N is chosen because it is an element that we have been discussing, although any metallicity-dependent element could be shown. In the left panel, the red arrow indicates the evolution along the low-Ia MW sequence, which formed in the early stages of the MW's history. The [(C+N)/Mg] abundance increases with increasing [Mg/H]. Then, at some point along this sequence, an infall of pristine gas would decrease the [Mg/H], but not change the [(C+N)/Mg] abundance, as indicated by the black arrow. The right panel

shows the same idea, but now the high-Ia MW stars are colored by Galactic cylindrical radius ( $R_{\rm cy}$ ), demonstrating that the high-Ia MW sequence is not necessarily a sequence in time, but can be a sequence that is populated by some combination of previously enriched gas mixed with some amount of pristine gas, the relative contribution of each apparently dependent on location in the Galaxy.

The point of this discussion is not necessarily to describe exactly what is happening in the MW, but to demonstrate that if there is a large amount of pristine inflow in the MW that occurs on relatively short timescales strong enough to significantly dilute ISM abundances, but this does not occur in the satellite galaxies, then we would expect the MW two-process model to fail on predicting any metallicity-dependent element in the satellite galaxies. The elements that are predicted well for the satellite galaxies when using the MW two-process model, as shown in the top panel of Figure 8, tend to be elements that are not metallicity dependent. A simple and fundamental difference such as pristine inflow would also explain why the DG twoprocess model is able to accurately predict the abundances of the satellite galaxies. However, given the different magnitude of the residuals from the MW two-process model, it is not clear if pristine inflow can explain all of the residuals. Future work that adds a "dilution" vector to the two-process model will help clarify the extent to which pristine inflow results in large residuals in the satellite galaxies when using the MW twoprocess model.

# 6.4. Outflows and IMF

In addition to the inflow of pristine gas, fundamental differences in outflows between the satellite galaxies and MW could explain some of the residuals, particularly the large underpredictions of C+N, Na, and Al. Being lower mass and, in some cases, in the process of disrupting, the satellite galaxies may not have been able to hold onto ejecta from SNe as effectively as the more massive MW. If such outflows were progenitor dependent, where ejecta from more massive SNe, were more likely to leave the system than less massive SNe, then we would expect deficiencies in elements that are produced in hydrostatic burning, the yields of which depend on the mass of the progenitor. Such differences in outflows would not be properly captured by the two-process model, and would result in large residuals of elements like C+N, Na, and Al, which is what we observe.

A different scenario, but with similar effects, is that star formation of the more recent populations of these stars occurred in a way that the most massive stars did not form, e.g., "top-light" IMF (e.g., A. McWilliam et al. 2013; S. Hasselquist et al. 2017; J. L. Carlin et al. 2018). If these massive stars never formed, then the mass-dependent hydrostatic elements would be produced in smaller quantities. To explore this idea, we use chemical evolution models generated using flexCE (B. H. Andrews et al. 2017) to analyze how a galaxy's [Al/Mg]–[Mg/H], [Na/Mg]–[Mg/H], [Ca/Mg]–[Mg/H], and [Si/Mg]–[Mg/H] abundance patterns change when the model contains an upper mass cutoff of 30 solar masses such that these stars are not formed and do not contribute to the chemical evolution of the galaxy (Figure 13). We only changed this upper mass cutoff, otherwise using the parameters of their fiducial model, which used CCSNe yields from M. Limongi & A. Chieffi (2006), AGB yields from A. I. Karakas et al. (2010), and SNe Ia yields from the W70 model of K. Iwamoto et al. (1999). We chose to analyze these four elements as they are among the best-fit elements to the MW.

From the top panel of Figure 8, we would expect the mass cutoff model to show relative deficiencies in Al and Na, slight enhancement in Ca, and no change in Si. This is qualitatively consistent with what we see in Figure 13 between the two models. [Ca/Mg] is enhanced only for the more chemically evolved stars, but recall that the MW two-process model can only be applied to the most chemically evolved satellite galaxy stars as that is where the samples overlap. The models also suggest that we should see small residuals in [Si/Mg], which we do not observe. Obviously these models ultimately depend on the yields, which are often uncertain, but a top-light IMF might be something that is revisited once a dilution vector is taken into account and better understood. The DG two-process model accurately predicting the elements for all satellite galaxies suggests that if the top-light IMF/mass-dependent outflows scenario were responsible for the MW two-process model residuals, then all satellite galaxies would have to have the same IMF/outflows, which is perhaps unexpected given the range of stellar masses and environments probed by these satellite galaxies.

# 6.5. Atypical SNe in the Satellite Galaxies

Another explanation of why the MW two-process model results in large satellite galaxy residuals for some elements and the DG two-process model does not is that fundamentally different types of SNe are occurring between the two types of galaxies. These could be for both CC and SNe Ia, but given that all of the Fe-peak elements aside from Cr are underpredicted, perhaps the satellite galaxies are primarily polluted by a different type of SNe Ia. A range of literature works (e.g., E. N. Kirby et al. 2019; C. Kobayashi et al. 2020b; M. A. C. Reyes et al. 2022) find that the abundance patterns of some of the dwarf spheroidal galaxies are most consistent with being polluted by sub-Chandrasekhar-mass SNe Ia. Figure 10 of M. A. C. Reyes et al. (2022) demonstrates that using sub-Chandrasekhar-mass SNe Ia yields from G. Y. C. Leung et al. (2020) and K. J. Shen et al. (2018) with their best-fit chemical evolution model of the Sculptor dSph galaxy results in [Mn/Fe] and [Ni/Fe] abundance ratios that are  $\sim$ 0.3–0.5 dex lower than with Chandrasekhar-mass SNe Ia yields. However, it is not clear if sub-Chandrasekhar-mass SNe Ia are not occurring in the MW, with a recent study by M. Palla (2021) demonstrating that a mixture of sub-Chandrasekhar-mass SNe Ia and Chandrasekhar-mass SNe Ia match the MW abundance trends. Still, perhaps it is this mixture that is different between the MW and satellite galaxies, or perhaps even more generally, the mixture is different depending on the metallicity, i.e., more metal-poor SNe Ia are more likely to be sub-Chandrasekhar mass.

For all satellite galaxies studied here, the maximum  $A_{\rm Ia}/A_{\rm CC}$  ratios (see Figure 4) occur at slightly different metallicities for each galaxy. Fornax and the SMC have a peak  $A_{\rm Ia}/A_{\rm CC}$  at [Mg/H]  $\sim$  -1.2, whereas Sgr has a peak  $A_{\rm Ia}/A_{\rm CC}$  ratio at [Mg/H]  $\sim$ -1.0 and a secondary peak at the most metal-rich stars. Moreover, the value of this ratio is much higher in Fnx than in Sgr, implying that at [Mg/H] = -1.2, SNe Ia dominated the chemical evolution of Fnx, and did so in a way that was unlike any of the other satellite galaxies. If different types of SNe Ia occurred at different metallicities, we might expect some of the Fe-peak elements to show residuals in the SMC, and

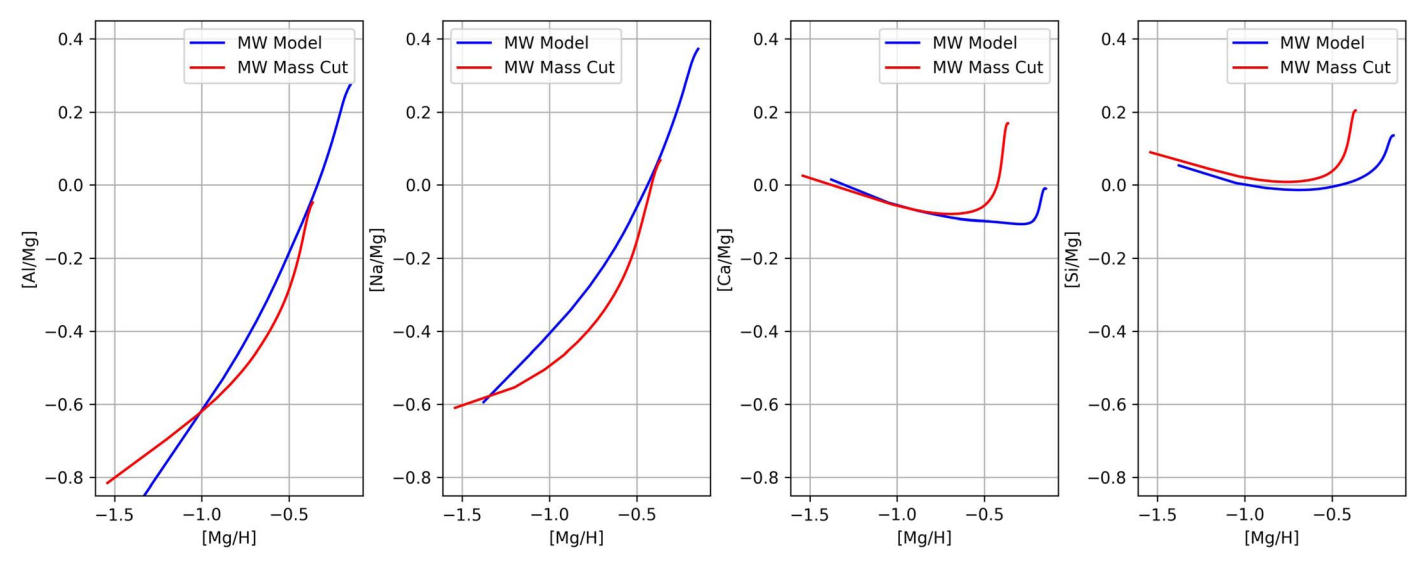


Figure 13. Chemical evolution tracks in [X/Mg]–[Mg/H] abundance space for four elements. Chemical evolution tracks are generated using flexCE, with the blue lines showing the chemical tracks from a fiducial MW model and the red lines showing the chemical tracks from a model with the same parameters except for a mass cutoff of  $30 M_{\odot}$  such that stars beyond this mass do not form.

especially Fnx, when using the DG two-process model to predict their abundances. The bottom panel of Figure 8 shows that, out of all the satellite galaxies, Fnx has the largest median residuals for Si, K, Ni, and Co, with the Ni residuals being the most significant given the small scatter relative to the magnitude of the median residual. Ni and Co have the largest residuals, and are elements produced in SNe Ia. However, Mn and Cr, elements that are also produced in large quantities by SNe Ia, do not show any residuals. Therefore, a metallicity-dependent SNe Ia explosion scenario would have to result in different Co and Ni, but not different Mn and Cr.

# 7. Summary and Conclusions

We have used two sets of stellar samples, low-Ia MW + high-Ia MW and low-Ia MW + high-Ia DG (Sgr), to derive two sets of abundance vectors for two separate two-process models, which we refer to as the MW two-process model and the DG two-process model. If we use the MW two-process model to predict the abundances of the more metal-rich ([Mg/H] > -0.8) stars of the LMC, Sgr, and GSE, we find that the model underpredicts the abundance of Ce by ~0.2 dex for the LMC and Sgr, and overpredicts the abundances of C+N, Na, Al, Ni, Mn, and Co for all three satellite galaxies. The MW two-process model also slightly underpredicts the abundance of Ca for these three satellite galaxies by  $\sim$ 0.1 dex. The MW two-process model accurately predicts the abundances of O, Si, K, and Cr. There are also residuals for S and V, but these are elements that are less precisely measured by APOGEE, and we do not consider them in the discussion.

Despite the apparent failure of the MW two-process model to predict many of the abundances of the satellite galaxies, if we use the abundances of Sgr to derive abundance vectors for a DG two-process model, we find that the abundances for all of the satellite galaxies are reasonably well-predicted by this model. This means that, despite the wide variation in observed abundance patterns for each element between the galaxies as highlighted by S. Hasselquist et al. (2021), each galaxy has the "expected" [X/Mg] abundance given its median [Fe/Mg] abundance at fixed [Mg/H]. Therefore, to the precision to which these abundances can be measured, the prompt and

delayed processes that enriched the gas in the satellite galaxies occurred in a very similar way, but one or more of these processes are fundamentally different from the satellite galaxies in the MW.

Regardless of the interpretation in terms of enrichment processes, one can view the two-process model as a way of comparing the multielement abundances of stellar populations that account for differences in overall metallicity and  $[\alpha/Fe]$  ratio. Our main empirical finding (Figure 8) is that after accounting for these differences, the abundance patterns of the remaining 14 elements investigated here are similar among the five dwarf satellites but different between these satellites and the MW disk.

We have considered a number of possible explanations for this difference, and the full explanation may be a mix of these and other mechanisms. The delayed contribution to Ce, and perhaps to other elements in our data set, is likely dominated by AGB stars rather than SNe Ia. The +0.2 dex residual for Ce in the LMC and Sgr implies that the ratio of AGB to Type Ia enrichment is higher in these systems than in the MW disk or GSE, for the common metallicity range. This differing ratio could arise from different SFHs, or perhaps from different relative retention of AGB and CC/SNe Ia products, or even from differences in binary star populations that lead to different numbers of SNe Ia per unit mass of star formation. We find tentative evidence that Al enrichment is more closely tied to C+N rather than Mg, so that whatever mechanism leads to lower C+N in the satellites also leads to lower Al.

Many of the elements that show large residuals are those that also have metallicity-dependent process vectors, which in turn reflect metallicity-dependent yields. Motivated by the two-infall scenario for MW chemical evolution (C. Chiappini et al. 1997; E. Spitoni et al. 2019), we hypothesize that a large inflow of pristine gas could have diluted the abundances of all elements in the ISM prior to the formation of the high-Ia, thin-disk population (Figure 12). In this case, the abundance ratios of low metallicity disk stars ([Mg/H]  $\approx$  -0.6) would be set by yields of a higher metallicity stellar population ([Mg/H]  $\approx$  0 -0.2), making them markedly different from those of DGs that reached [Mg/H] $\approx$  -0.6 near the end of their evolution. This

scenario could be investigated more thoroughly in future studies by extending the two-process model to allow for dilution and searching for signatures of this effect in disk populations of different ages, metallicities, and locations.

All of these explanations assume that the IMF-averaged yields of CCSNe and SNe Ia are the same between the DGs and the MW. Another possibility is that these averaged yields are themselves different, even at the same metallicity, perhaps because of different IMF slopes or different ratios of sub-Chandrasekhar-mass to Chandrasekhar-mass progenitors of SNe Ia. This scenario requires a systematic difference between the MW and its satellites but close consistency among the satellites themselves—only Fnx shows residuals relative as large as 0.1 dex for multiple elements (Ni, Co, Ce, and the less reliably measured Na) relative to the other DGs. The impact of IMF changes could be studied with theoretical yield calculations to predict multielement signatures of this effect, and differences in SNe Ia yields could be tested by focusing on

elements whose production is most sensitive to progenitor properties. If some of the chemical differences between the MW and its satellites can be conclusively tied to different yields, they will imply a remarkable connection between stellar-scale astrophysics and galactic-scale environment.

# Appendix Results from the log g-matched MW Sample

In Section 2, we discuss using a  $T_{\rm eff}$ -matched MW sample as well as a log g-matched sample. Figure 1 shows that when we match one of these parameters, the distribution of the other parameter does differ from the distribution of the satellite galaxies. We have primarily focused the results and discussion on the  $T_{\rm eff}$ -matched MW sample, but we show in Figure 14 that the residual abundance patterns we get from deriving two-process model parameters from the log g-matched sample are nearly identical to the results from the  $T_{\rm eff}$ -matched MW sample.

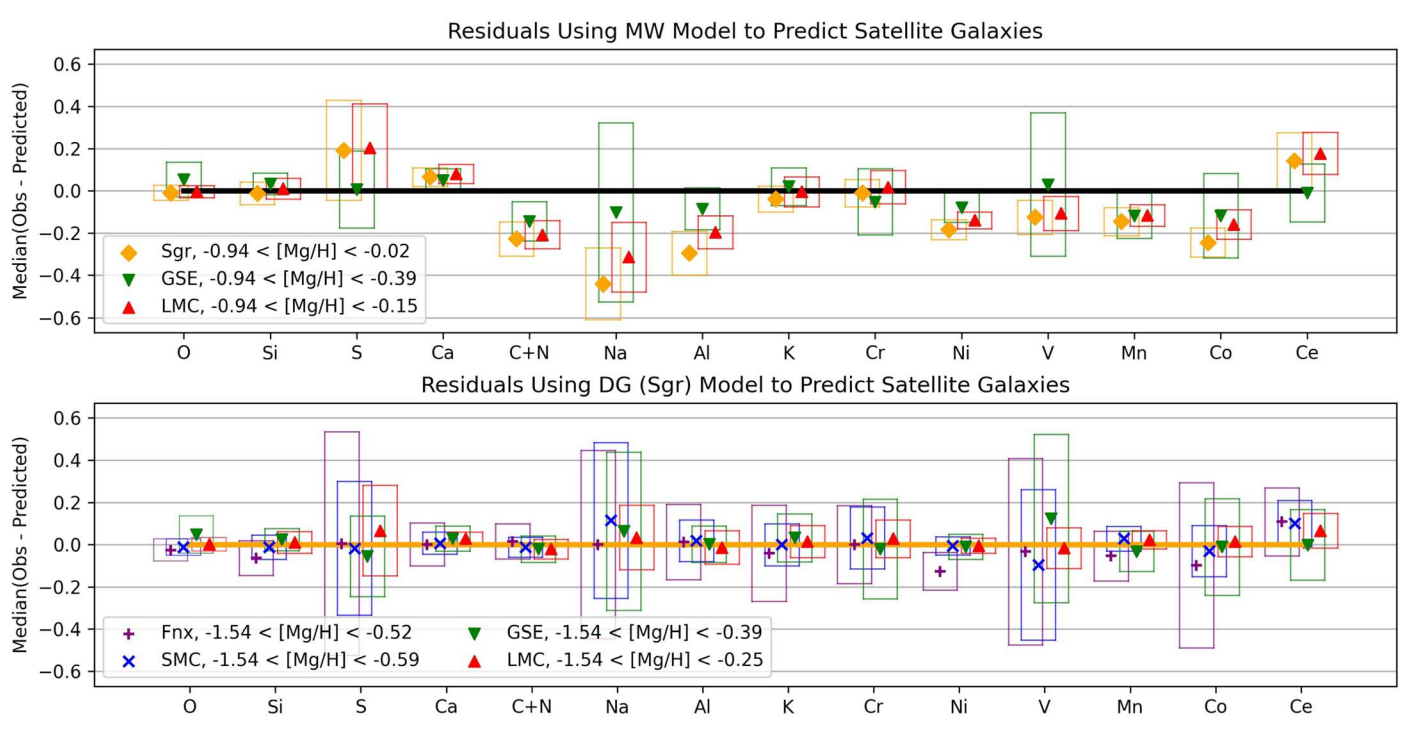


Figure 14. Same as Figure 8 but for the  $\log g$ -matched MW sample instead of the  $T_{\text{eff}}$ -matched MW sample.

#### ORCID iDs

Sten Hasselquist https://orcid.org/0000-0001-5388-0994 Christian R. Hayes https://orcid.org/0000-0003-2969-2445 Emily J. Griffith https://orcid.org/0000-0001-9345-9977 David Weinberg https://orcid.org/0000-0001-7775-7261 Tawny Sit https://orcid.org/0000-0001-8208-9755 Rachael L. Beaton https://orcid.org/0000-0002-1691-8217 Danny Horta https://orcid.org/0000-0003-1856-2151

#### References

```
Abdurro'uf, Accetta, K., Aerts, C., et al. 2022, ApJS, 259, 35
Allende Prieto, C., Beers, T. C., Wilhelm, R., et al. 2006, AJ, 636, 804
Andrews, B. H., Weinberg, D. H., Schönrich, R., & Johnson, J. A. 2017, ApJ,
Beaton, R. L., Oelkers, R. J., Hayes, C. R., et al. 2021, AJ, 162, 302
Belokurov, V., Erkal, D., Evans, N. W., Koposov, S. E., & Deason, A. J. 2018,
   MNRAS, 478, 611
Blanton, M. R., Bershady, M. A., Abolfathi, B., et al. 2017, AJ, 154, 28
Bowen, I. S., & Vaughan, A. H. 1973, ApOpt, 12, 1430
Brown, A. G. A., Vallenari, A., Prusti, T., & de Bruijne, J. H. J. 2018, A&A,
Buck, T., Obreja, A., Ratcliffe, B., et al. 2023, MNRAS, 523, 1565
Buder, S., Sharma, S., Kos, J., et al. 2021, MNRAS, 506, 150
Carlin, J. L., Sheffield, A. A., Cunha, K., & Smith, V. V. 2018, ApJL, 859, L10
Chiappini, C., Matteucci, F., & Gratton, R. 1997, ApJ, 477, 765
Ciuca, I., Kawata, D., Ting, Y.-S., et al. 2024, MNRAS, 528, L122
Cunha, K., Smith, V. V., Hasselquist, S., et al. 2017, ApJ, 844, 145
Deason, A. J., Belokurov, V., Koposov, S. E., & Lancaster, L. 2018, ApJL,
   862, L1,
Edvardsson, B., Andersen, J., Gustafsson, B., et al. 1993, A&A, 275, 101
Eisenstein, D. J., Weinberg, D. H., Agol, E., et al. 2011, AJ, 142, 72
García Pérez, A. E., Allende Prieto, C., Holtzman, J. A., et al. 2016, AJ,
   151, 144
Griffith, E., Weinberg, D. H., Johnson, J. A., et al. 2021, ApJ, 909, 77
Griffith, E. J., Hogg, D. W., Dalcanton, J. J., et al. 2024, AJ, 167, 98
Griffith, E. J., Johnson, J. A., Weinberg, D. H., et al. 2023, ApJ, 944, 47
Griffith, E. J., Weinberg, D. H., Buder, S., et al. 2022, ApJ, 931, 23
Gunn, J. E., Siegmund, W. A., Mannery, E. J., et al. 2006, AJ, 131, 2332
Hasselquist, S., Hayes, C. R., Lian, J., et al. 2021, ApJ, 923, 172
Hasselquist, S., Holtzman, J. A., Shetrone, M., et al. 2019, ApJ, 871, 181
Hasselquist, S., Shetrone, M., Smith, V., et al. 2017, ApJ, 845, 162
Hayden, M. R., Bovy, J., Holtzman, J. A., et al. 2015, ApJ, 808, 132
Hayes, C. R., Majewski, S. R., Shetrone, M., et al. 2018, ApJ, 852, 49
Helmi, A., van Leeuwen, F., McMillan, P., et al. 2018, A&A, 616, A12
Hendricks, B., Koch, A., Lanfranchi, G. A., et al. 2014, ApJ, 785, 102
Iwamoto, K., Brachwitz, F., Nomoto, K., et al. 1999, ApJS, 125, 439
Ji, A. P., Frebel, A., Simon, J. D., & Chiti, A. 2016, ApJ, 830, 93
Ji, A. P., Li, T. S., Simon, J. D., et al. 2020, ApJ, 889, 27
Jönsson, H., Holtzman, J. A., Allende Prieto, C., et al. 2020, AJ, 160, 120
Karakas, A. I., Campbell, S. W., & Stancliffe, R. J. 2010, ApJ, 713, 374
```

Kirby, E. N., Xie, J. L., Guo, R., et al. 2019, ApJ, 881, 45

Kobayashi, C., Karakas, A. I., & Lugaro, M. 2020a, ApJ, 900, 179

Kobayashi, C., Leung, S.-C., & Nomoto, K. 2020b, ApJ, 895, 138

```
Kobayashi, C., Umeda, H., Nomoto, K., Tominaga, N., & Ohkubo, T. 2006,
   ApJ, 653, 1145
Koch, A., McWilliam, A., Grebel, E. K., Zucker, D. B., & Belokurov, V. 2008,
  ApJL, 688, L13
Leung, G. Y. C., Leaman, R., van de Ven, G., & Battaglia, G. 2020, MNRAS,
  493, 320
Leung, H. W., & Bovy, J. 2019, MNRAS, 483, 3255
Lian, J., Storm, N., Guiglion, G., et al. 2023, MNRAS
Lian, J., Zasowski, G., Hasselquist, S., et al. 2020, MNRAS, 500, 282
Limongi, M., & Chieffi, A. 2006, ApJ, 647, 483
Loebman, S. R., Debattista, V. P., Nidever, D. L., et al. 2016, ApJL,
  818, L6
Mackereth, J. T., Bovy, J., Schiavon, R. P., et al. 2017, MNRAS, 471, 3057
Majewski, S. R., Schiavon, R. P., Frinchaboy, P. M., et al. 2017, AJ, 154, 94
McWilliam, A., Piro, A. L., Badenes, C., & Bravo, E. 2018, ApJ, 857, 97
McWilliam, A., Wallerstein, G., & Mottini, M. 2013, ApJ, 778, 149
Nidever, D. L., Bovy, J., Bird, J. C., et al. 2014, ApJ, 796, 38
Nidever, D. L., Hasselquist, S., Hayes, C. R., et al. 2020, ApJ, 895, 88
Nidever, D. L., Holtzman, J. A., Allende Prieto, C., et al. 2015, AJ, 150, 173
Nissen, P. E., & Schuster, W. J. 2010, A&A, 511, L10
Osorio, Y., Allende Prieto, C., Hubeny, I., Mészáros, S., & Shetrone, M. 2020,
   A&A, 637, A80
Palla, M. 2021, MNRAS, 503, 3216
Prantzos, N., Abia, C., Cristallo, S., Limongi, M., & Chieffi, A. 2020,
      NRAS, 491, 1832
Ratcliffe, B. L., & Ness, M. K. 2023, ApJ, 943, 92
Reyes, M. A. C., Kirby, E. N., Ji, A. P., & Nuñez, E. H. 2022, ApJ, 925, 66
Rybizki, J., Just, A., & Rix, H.-W. 2017, A&A, 605, A59
Salaris, M., Pietrinferni, A., Piersimoni, A. M., & Cassisi, S. 2015, A&A,
  583. A87
Santana, F. A., Beaton, R. L., Covey, K. R., et al. 2021, AJ, 162, 303
Schiavon, R. P., Phillips, S. G., Myers, N., et al. 2024, MNRAS, 528, 1393
Schönrich, R., & Binney, J. 2009, MNRAS, 399, 1145
Sheinis, A., Anguiano, B., Asplund, M., et al. 2015, JATIS, 1, 035002
Shen, K. J., Kasen, D., Miles, B. J., & Townsley, D. M. 2018, ApJ, 854, 52
Shetrone, M., Venn, K. A., Tolstoy, E., et al. 2003, AJ, 125, 684
Sit, T., Weinberg, D. H., Wheeler, A., et al. 2024, ApJ, 970, 180
Sneden, C., Cowan, J. J., & Gallino, R. 2008, ARA&A, 46, 241
Spitoni, E., Matteucci, F., Gratton, R., et al. 2024, arXiv:2405.11025
Spitoni, E., Silva Aguirre, V., Matteucci, F., Calura, F., & Grisoni, V. 2019,
       . 623, A60
Ting, Y.-S., & Weinberg, D. H. 2022, ApJ, 927, 209
Tinsley, B. M. 1979, ApJ, 229, 1046
Truran, J. W., & Arnett, W. D. 1971, Ap&SS, 11, 430
Weinberg, D. H., Holtzman, J. A., Hasselquist, S., et al. 2019, ApJ,
  874, 102
Weinberg, D. H., Holtzman, J. A., Johnson, J. A., et al. 2022, ApJS, 260, 32
Wilson, J. C., Hearty, F. R., Skrutskie, M. F., et al. 2019, PASP, 131,
  055001
Woosley, S. E., Wilson, J. R., Mathews, G. J., Hoffman, R. D., & Meyer, B. S.
   1994, ApJ, 433, 229
Zamora, O., García-Hernández, D. A., Allende Prieto, C., et al. 2015, AJ,
  149, 181
Zasowski, G., Cohen, R. E., Chojnowski, S. D., et al. 2017, AJ, 154, 198
Zasowski, G., Johnson, J. A., Frinchaboy, P. M., et al. 2013, AJ, 146, 81
Zasowski, G., Schultheis, M., Hasselquist, S., et al. 2019, ApJ, 870, 138
```